The 16th Symposium on Polar Science

2－5 December 2025

National Institute of Polar Research

Research Organization of Information and Systems

Session OM

Polar Meteorology and Glaciology

Abstracts

Conveners: Shun Tsutaki, and Yutaka Tobo (NIPR)

Measurement of Sea Ice Thickness and Floe Using UAV-LiDAR

Hayate Kato[1], Kazutaka Tateyama[2], Hidekazu Shirai[2] and Yuki Shimura[1]
[1]*Graduate School of Engineering, Kitami Institute of Technology, Kitami, Japan*
[2]*School of Earth, Energy and Environmental Engineering,*
Kitami Institute of Technology, Kitami, Japan

The Arctic research vessel Mirai II, under construction by JAMSTEC and scheduled for completion in autumn 2026, is designed to include “non-destructive sea-ice monitoring using autonomous aerial and underwater observation drones” as a future observational capability. Moreover, rapid and precise sea ice condition assessment is essential for vessels navigating polar regions to select safe routes.

Traditionally, sea-ice surveys with unmanned aerial vehicles (UAVs) have relied entirely on photogrammetry based on Structure-from-Motion (SfM) techniques (UAV-SfM). One of the challenges of Structure-from-Motion (SfM) is that it relies entirely on natural light, making observations infeasible at night or during snowfall and rainfall. Furthermore, in order to obtain three-dimensional positional information, overlapping imagery is indispensable; however, the accuracy of measurements was insufficient for drift ice that moved during image acquisition. In addition, the vertical accuracy depended on the availability of Ground Control Points (GCPs), which could introduce errors in the absolute accuracy.

In this study, we introduced a new approach by equipping a UAV with LiDAR (UAV-LiDAR) to address these challenges and conducted sea-ice observations. Unlike optical sensors, LiDAR employs an active laser source, which is unaffected by natural light conditions and enables the direct acquisition of three-dimensional positional information of target objects. Field experiments were conducted in February 2025 on drift ice grounded off Utoro, Hokkaido, and on the frozen surface of Lake Saroma, Hokkaido, using a DJI MATRICE 350 RTK platform equipped with a DJI Zenmuse L2 LiDAR sensor and supported by a D-RTK 2 Mobile Station base station.

As a result, the surface of the sea ice and the snow cover could be observed with sufficient accuracy (Fig1). Furthermore, with respect to the morphology of ice floes, edge detection enabled high-precision estimation of their diameters and areas(Fig2).

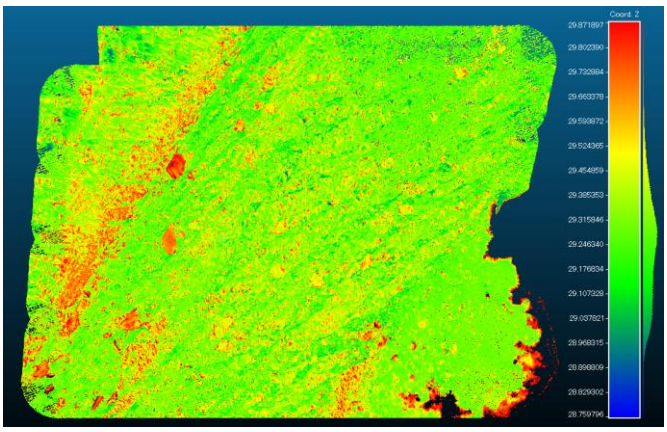

Figure 1. Thickness distribution of the sea-ice surface along the Utoro coast.

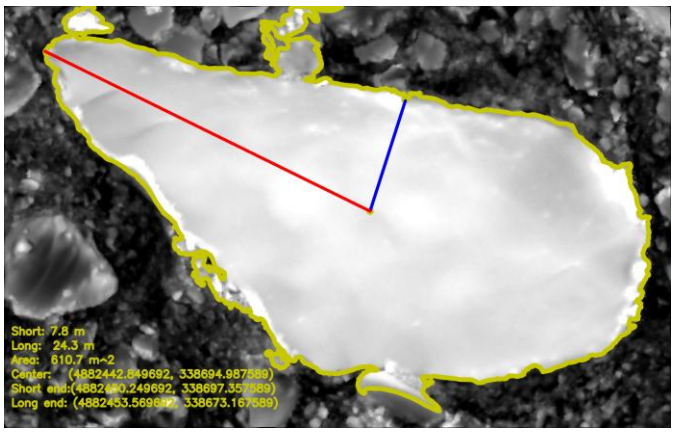

Figure 2. Edge-detection image of a floe

References

Watanabe, T.& Tateyama,K.(2021). An attempt to measure sea ice freeboard using UAV-SfM. Seppyo 83 (2), 155-167.

Comparison between in-situ and satellite observations of Arctic sea ice

Kazutaka Tateyama[1], Shotaro Muraoka[2] and Midori Nagao[1]
[1]*School of Earth, Energy and Environmental Engineering, Kitami Institute of Technology, Kitami, Japan*
[2]*Graduate School of Engineering, Kitami Institute of Technology, Kitami, Japan*

Since the 1980s, both the extent and thickness have declined thorough year. Most multi-year ice has been lost, and the sea ice distribution has shifted to a new state in which first-year ice accounts for more than three-quarters. The wintertime recovery capacity has also weakened, and then making the thinner (ICCI, 2023).

This study aims to conduct ground validation of sea ice observations using a JAXA's new satelliteborne passive microwave radiometer AMSR3 onboard the GOSAT-GW satellite, launched in 2025, high resolution brightness temperatures (5km) from AMSR2 onboard GCOM-W were compared with in-situ sea ice observations collected in the Canada Basin during Auguast - September 2024 and September - October 2025. In parallel, toward future deployment on the Arctic research vessel Mirai II, sea ice products observed from an automated sea ice information acquisition system integrating a Shipborne Sea Ice Condition Recorder (SSICR), Shipborne Electro-Magnetic induction ice thickness profiler (SEM), a portable passive microwave radiometer and a LiDAR was compared with visual sea ice observations by observers. The SEM provides ice concentration and total (sea ice + snow) thickness estimates by exploiting the conductivity contrast between sea ice and seawater (Haas, 1998), while SSICR and LiDAR enables high-resolution surface and floe-edge morphology mapping.

Figure 1 shows the distribution of high-resolution AMSR2-derived sea ice concentration in the Canada Basin in September 2024. Figure 2 presents a comparison between sea ice concentration that accounts for the total ice thickness observed by SEM and the AMSR2-derived sea ice concentration. Sea ice concentration from AMSR2 showed a tendency to be biased low for thin ice and biased high for thick ice.

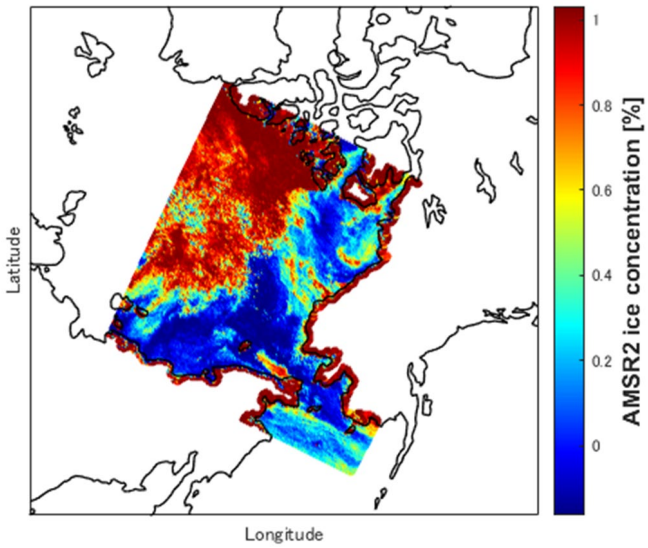

Figure 1. Sea ice concentration distribution in 2024 of the Canada Basin in September using high-resolution AMSR2 brightness temperature data.

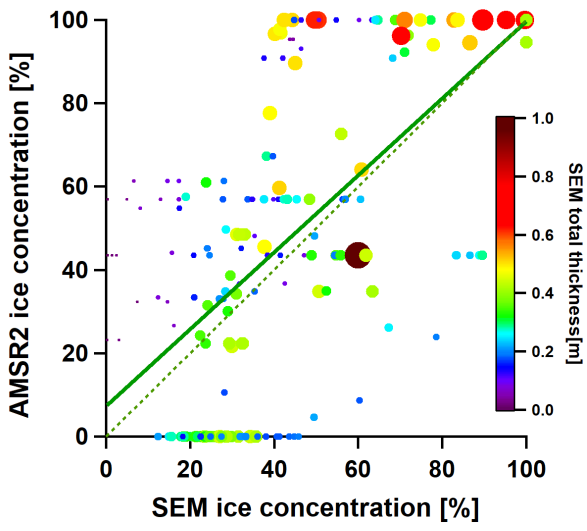

Figure 2. Comparison of sea ice concentration measured by SEM and AMSR2 with accounting total thickness defference.

References

International Cryosphere Climate Initiative (ICCI). State of the Cryosphere 2023: Two Degrees Is Too High. Nov. 2023, https://www.iccinet.org/statecryo23.

Haas, C. Evaluation of ship-based electromagnetic-inductive thickness measurements of summer sea-ice in the Bellingshausen and Amundsen Seas, Antarctica, Cold Regions Science and Technology, 27(1), 1-16, 1998 10.1016/S0165-232X(97)00019-0.

Antarctic sea ice multidecadal variability triggered by Southern Annular Mode and deep convection

Yushi Morioka[1], Syukuro Manabe[2], Liping Zhang[3,4], Thomas L. Delworth[3], William Cooke[3], Masami Nonaka[1], Swadhin Behera[1]
[1]*Application Laboratory, VAiG, JAMSTEC*
[2]*Atmospheric and Oceanic Sciences Program, Princeton University*
[3]*Geophysical Fluid Dynamics Laboratory, NOAA*
[4]*University Corporation for Atmospheric Research*

Antarctic sea ice exerts great influence on Earth's climate by controlling the exchange of heat, momentum, freshwater, and gases between the atmosphere and ocean. Satellite observation shows that Antarctic sea ice extent has undergone a multidecadal increase followed by a substantial decline since 2016. Here we utilize a 300-year sea ice reconstruction data and several thousand years of two NOAA/GFDL and five CMIP6 model simulations to demonstrate a multidecadal variability of Antarctic sea ice extent. Stronger westerlies associated with the Southern Annular Mode (SAM), an atmospheric intrinsic variability in the Southern Hemisphere, enhance the upwelling of warm and saline water from the subsurface ocean. The consequent salinity increase in the upper ocean weakens the near-surface stratification, induces deep convection, and in turn brings more subsurface warm and saline water to the surface. The positive feedback between ocean salinity and deep convection triggered by the SAM provides favorable conditions for a multidecadal sea ice decrease in the Antarctic Sea. Processes acting in reverse are found to cause a multidecadal sea ice increase, although it evolves more slowly than the sea ice decrease.

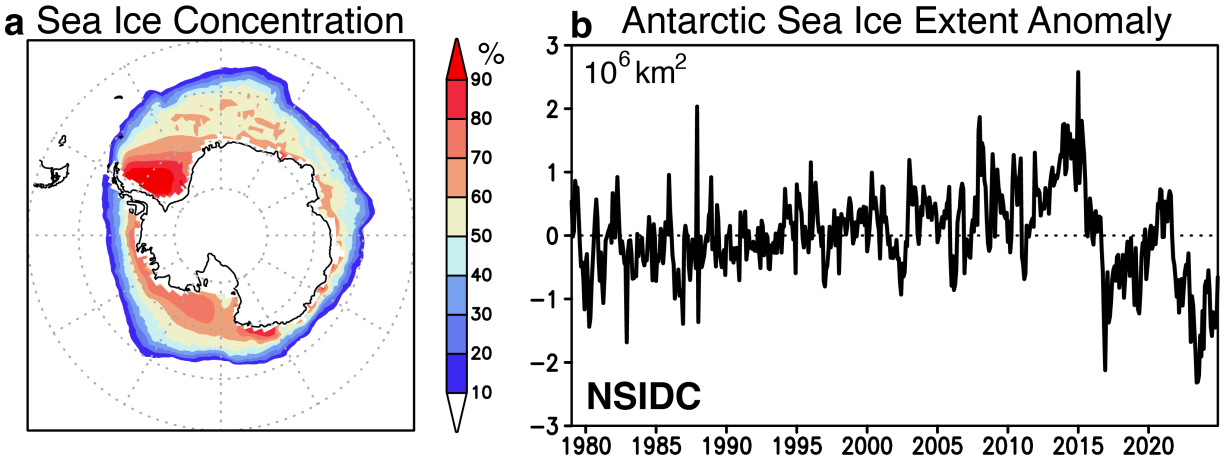

Figure 1: Observed Antarctic sea ice during 1979-2024. **a**, Annual mean of Antarctic sea ice concentration (color in %) during 1979-2024 from NSIDC. **b**, Time series of monthly Antarctic SIE anomaly (black in 10^6 km^2) during 1979-2024 from NSIDC. Here we defined the monthly anomaly as a deviation from the monthly climatology during 1979-2024 after removing a linear trend. A dashed line indicates a zero line.

References

Morioka, Y., Manabe, S., Zhang, L., Delworth, T. L., Cooke, W., Nonaka, M., & Behera, S. K. (2024a). Antarctic sea ice multidecadal variability triggered by Southern Annular Mode and deep convection. Communications Earth & Environment, 5, 633, https://doi.org/10.1038/s43247-024-01783-z.

Morioka, Y., Zhang, L., Cooke, W., Nonaka, M., Behera, S. K., & Manabe, S. (2024b). Role of anthropogenic forcing in Antarctic sea ice variability simulated in climate models. Nature Communications, 15, 10511, https://doi.org/10.1038/s41467-024-54485-7

Response of the Antarctic coastal ocean–cryosphere system to ±6°C temperature anomalies

Kazuya Kusahara[1] and Hiroaki Tatebe[1]
[1]*Japan Agency for Marine-Earth Science and Technology (JAMSTEC)*

The Antarctic cryosphere has been undergoing significant changes in the ongoing global warming. Two major Antarctic cryosphere processes of ice shelves and sea ice strongly interact with the Southern Ocean. In this study, we investigate how these cryosphere–ocean processes respond to atmospheric warming using a coupled sea ice–ocean model with an ice-shelf component. We performed a series of numerical experiments by applying air temperature anomalies ranging from −6°C to +6°C, envisioning conditions from glacial to interglacial periods. The model results show that winter sea-ice extent and coastal sea-ice production respond almost linearly to the warming, while summer sea-ice extent diminishes to reach a lower limit. In contrast, ice-shelf basal melting exhibits a super-linear response, driven by increased contributions from two warm water masses: Antarctic Surface Water and Circumpolar Deep Water. This suggests that under warmer conditions, the response of Antarctic ice shelves may be much larger than previously understood, highlighting the need for a more nuanced understanding of ice-shelf basal melting under future warming scenarios. In addition, the meridional overturning circulation weakens as warming increases, and the core of dense-water formation originating from the Antarctic coastal region shifts toward lighter water masses. The impact of ice-shelf meltwater on the overturning circulation becomes more pronounced under warmer conditions, whereas under colder conditions the effect is relatively small. These results indicate that nonlinear responses and process interactions are critical in the Southern Ocean's deep-ocean circulation adjustment to temperature changes, underscoring the importance of their accurate representation in future prediction models.

OMo5

The δ15N of chlorophyll to reconstruct the nutrient cycle in the Adélie Basin, East Antarctica, over the last 2000 years

Thibault SUTRE [1,*], Johan ETOURNEAU [1,2], Xavier CROSTA [1], Nanako OGAWA[3], Chisato YOSHIKAWA[3], Hisami SUGA[3], Naohiko OHKOUCHI [3]

[1] *EPOC, UMR-CNRS 5805, Université de Bordeaux, 33615 Pessac, France*
[2] *EPHE/PSL Research University, 75014 Paris, France*
[3] *Biogeochemistry Research Center, JAMSTEC, Yokosuka, 237-0061, Japan*

* *Correspondence: thibault.sutre@u-bordeaux.fr*

The Southern Ocean plays a key role in global biogeochemical cycles. It particularly influences the nitrogen cycle through primary productivity and the redistribution of nutrients to lower latitudes. Although nitrates, the main source of bioavailable nitrogen, are generally abundant there, phytoplankton blooms linked to the seasonal sea ice cycle quickly deplete this stock in surface waters over the Antarctic continental shelf. However, observations of the nitrogen cycle in this area and of the processes that control it remain scarce. Paleo reconstructions are therefore needed to better understand how it will evolve later in a warming ocean.

The goal of our study is to investigate nitrogen cycle variability over the past two millennia. We aim to characterize its links with sea ice cover, ocean circulation, and primary productivity. To do this, we present the first use of $\delta^{15}N$ of chlorophyll ($\delta^{15}N_{chl}$) in the Antarctic coastal zone to study the nitrate cycle. Unlike traditional methods such as the $\delta^{15}N$ from the bulk, the $\delta^{15}N_{chl}$ is not sensitive to sedimentary diagenesis [1]. It can thus reliably record changes in the relative consumption of nitrate in the surface layer of the ocean.

We measured $\delta^{15}N_{chl}$ on a sediment core from IODP site U1357B (66°24.79'S–140°25.57'E), in Adélie Land, East Antarctica (Fig 1). Based on comparisons with independent data from both a nitrogen isotope model [2] and several proxies from the same core, we show that $\delta^{15}N_{chl}$ variations are due to changes in mixing depth. These changes control the supply of deep sources of nitrate, such as the nutrient rich mCDW (*modified* Circumpolar Deep Water), to surface waters. A multi-proxy approach also highlights how these nutrient supplies are influenced by sea ice dynamics.

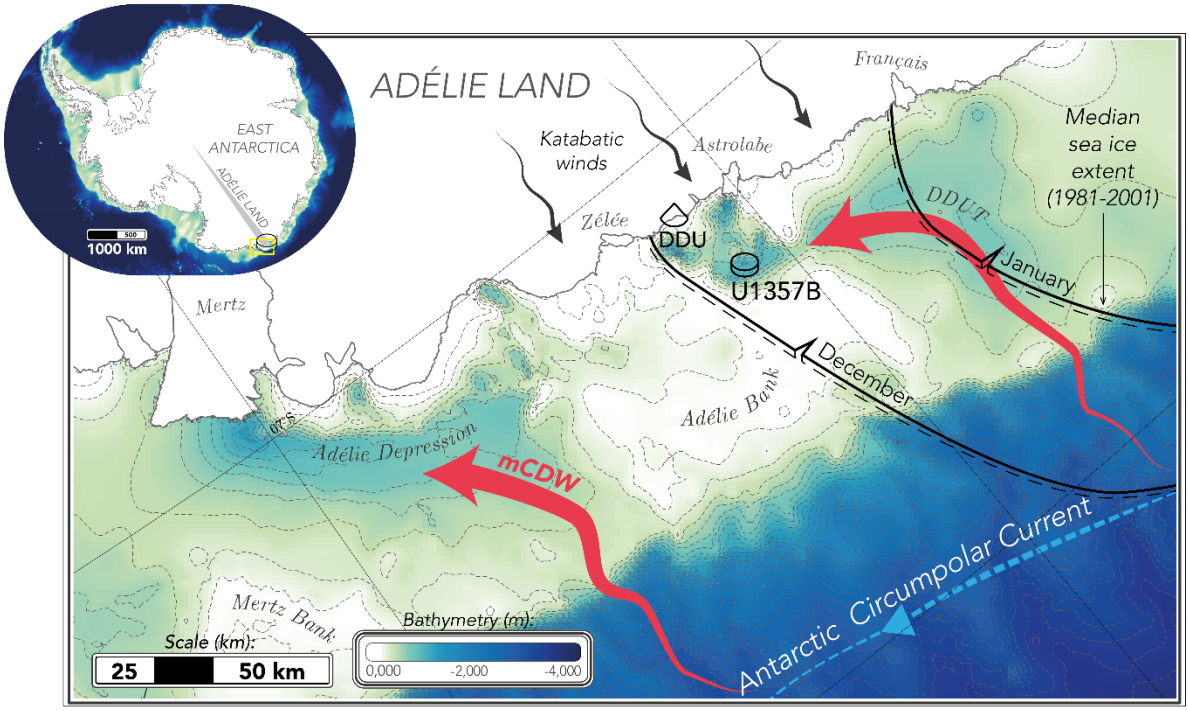

Figure 1. Location map of the study (mCDW = *modified* Circumpolar Deep Water, DDU = Dumont d'Urville station) [3]

Our study shows that the nitrogen cycle is not primarily influenced by primary productivity changes in the coastal waters of Antarctica. Instead, backed by the model outputs, we shed light on the influence of sea-ice seasonality on $\delta^{15}N_{chl}$ variations, with reduced (important) sea-ice presence in early summer linked to lower (higher) values of $\delta^{15}N_{chl}$. In other words, earlier and more rapid sea-ice break-up potentially enable more events of resupply due to a more effective wind stress on the ice-free summer surface layer. Such conditions lead to deep mixed layer depths and renewing of fresh $^{14}NO_3^-$ into the nutrient pool, as observed in the lower $\delta^{15}N_{chl}$ values. The $\delta^{15}N_{chl}$ signal therefore reflects environmental and oceanic conditions that govern mixing in the water column and upwelling of nutrients.

References: [1] Kashiyama et al. (2008) Science 321, 658–658. https://doi.org/10.1126/science.1158761 [2] Yoshikawa et al. (2005) J Oceanogr 61, 921–942. https://doi.org/10.1007/s10872-006-0010-5 [3] Matsuoka et al. (2021) Env. Mod. & Soft. 140 https://doi.org/10.1016/j.envsoft.2021.105015

OMo6

Particle distribution in the old sediment-laden sea ice in the Arctic Ocean

Keigo D. Takahashi[1], Emiliano Cimoli[1], Dmitry Divine[2], Sarah Lena Eggers[3], Thomas Krumpen[3], Morten Iversen[3], Julia Pamphile dos Santos[3], Daiki Nomura[1], and Marcel Nicolaus[3]
[1]*Faculty of Fisheries Sciences, Hokkaido University*
[2]*Norwegian Polar Institute*
[3]*Alfred Wegener Institute*

Sediment-laden sea ice (also known as dirty ice) is widely observed in the Arctic ocean. Sea ice formed in shallow coastal regions could incorporate suspended particles (Ito et al., 2019) and the release of lithogenic particles and nutrient could enhance particulate flux in offshore waters (Swoboda et al., 2024). Therefore, it is important to understand the mechanism and distribution of sediment-laden sea ice. Recent study using satellite ocean color could detect the spatial distribution of sediment-laden sea ice in the Arctic ocean (Waga et al., 2022). However, little studies have reported the sediment concentration in old (second or multiyear) pack ice, which is difficult to detect by remote sensing due to overlying snow. This study presents the particle concentration and physical characteristics of the older sediment-laden sea ice.

Sea-ice cores (up to 148 cm thick) were collected using a 14 cm-diameter Kovacs corer off Greenland in July and August of 2025 during the expedition aboard RV Polarstern (CONTRASTS, PS149). One sea-ice core was cut in half along it vertical axis and one half was thin sectioned vertically to determine the sea-ice growth history. The other half was divided into horizontal sections of 10 to 20 cm height and melted directly to measure the sediment concentration (turbidity) and salinity.

Sea-ice salinity ranged 0.0–3.1 and was <2.0 in the top 0–90 cm, suggesting that the ice was second or multiyear sea-ice that had undergone melting accompanied by brine release. Turbidity ranged 2.3–380.9 FTU and well defined peaks in turbidity was observed in the top 0–10 cm and 14–24 cm and an additional peaks in interior part of the sea-ice at 54–64 cm and 80–90 cm. The observations of multiple depth-layers containing sediments is in contrast to first-year ice, which typically only has one single dirty (sediment) layer (Wegner et al., 2017). The thin sections revealed that high-turbidity depth-layers corresponded with granular textures, corroborating that suspension of sediments and frazil ice interaction enhanced particle incorporation into sea ice. These results suggest that sediment-laden sea ice in offshore ice regions has more complex history, such as melting and rafting of floes, that affects the vertical distribution of sediment within sea ice. This further complicated predictions of impact from sediment release into the water column from melting sea ice, which has implications for both fertilization of the surface ocean and the ballasting effect of sediment on settling organic aggregates and particles.

References

Ito M, Ohshima KI, Fukamachi Y, Hirano D, Mahoney AR, Jones J, Takatsuka T, Eicken H, Favorable conditions for suspension freezing in an Arctic coastal polynya. 124(12), 8701-8719, 2019. Journal of Geophysical Research: Oceans, 10.1029/2019JC015536

Swoboda S, Krumpen T, Nöthig EM, Metfies K, Ramondenc S, Wollenburg J, Fahl K, Peeken I, Iversen M. Release of ballast material during sea-ice melt enhances carbon export in the Arctic Ocean. 3(4), pgae081, 2024. PNAS Nexus, 10.1093/pnasnexus/pgae081

Waga H, Eicken H, Light B, Fukamachi, Y, A neural network-based method for satellite-based mapping of sediment-laden sea ice in the Arctic. 270, 112861, 2022. Remote Sensing of Environment, 10.1016/j.rse.2021.112861

Wegner C, Wittbrodt K, Hölemann JA, Janout MA, Krumpen T, Selyuzhenok V, Novikhin A, Polyakova Ye, Krykova I, Kassens H, Timokhov L, Sediment entrainment into sea ice and transport in the Transpolar Drift: A case study from the Laptev Sea in winter 2011/2012. 141, 1-10, 2017. Continental Shelf Research, https://doi.org/10.1016/j.csr.2017.04.010

OMo7

Increased Frequency of Extratropical Cyclones in the Bering Strait and Chukchi Sea Region Under the Progression of Global Warming

Masatake E. Hori[1], Masakazu Yoshimori[1]
[1]*Atmosphere and Ocean Research Institute, The University of Tokyo, Kashiwa, Japan*

Extratropical cyclones (ETCs) are a fundamental component of climate in the midlatitudes and the Arctic, strongly influencing the distribution of precipitation and governing the poleward transport of heat and moisture. Utilizing an idealized GCM, Tamarin and Kaspi (2017) found that both the location of cyclogenesis and the movement of individual ETCs shift northward under global warming. Crawford et al. (2023) also studied the change in propagation of ETCs using multiple CMIP models under projected global warming and revealed a seasonal and regional dependence of ETC tracks associated with the mean difference in tropospheric thickness. Here, we focus on the wintertime northern North Pacific, particularly the northern flank of the mean storm track near the Bering Strait, where extreme ETCs are known to cross into the Chukchi Sea, to investigate how the propagation properties change under the global warming conditions.

The dataset used is the Database for Policy Decision-Making for Future Climate Change (d4PDF; Mizuta et al. 2017), which is a large ensemble AGCM dataset designed to quantify the response in atmospheric processes to changing states of greenhouse gases and sea surface temperature as well as sea-ice boundaries. We use the 30-year daily sea level pressure data and other variables from the non-warming simulation (HPB-NAT), which consists of 100 members, to compare them against the 2K and 4K warming experiments (HFB-2K and 4K) with 54 and 90 members, respectively. To objectively track each cyclone, we utilize the cyclone detection and tracking algorithm developed by the University of Melbourne (Murray and Simmonds 1991), in which the detection parameters are optimized by comparing the output to the CEOS/NSIDC extratropical cyclone tracking dataset (Crawford et al. 2021) under the ERA5 atmospheric reanalysis dataset (Hersbach et al. 2017).

While the number of cyclone systems in the North Pacific basin decreased under the HFB-4K experiment by 6.5% compared to the HPB-NAT experiment, the number of cyclones passing through the Bering Strait increased by 32% under HFB-4K experiment. ETCs passing through the Bering Strait show an increased tendency of northward movement characterized by an 18˚ eastward displacement in the average cyclogenesis location and a 10˚ westward displacement in the average cyclolysis location. The maximum Eady growth rate, which quantifies the baroclinic instability of the atmosphere, shows a positive signature in the lower troposphere over the northern North Pacific as well as the Chukchi Sea, coinsiding with the region with increased frequency of ETCs. In our presentation, we will further explore the difference in mean cyclone propagation pathways and the atmospheric environment in which the cyclones intensify.

References

Crawford AD et al. CEOS/NSIDC Extratropical Cyclone Tracking (CNECT)", DOI, CanWIN, Version 13.2., 2021.

Crawford AD, McCrystall MR, Lukovich JV, Stroeve JC, The Response of Extratropical Cyclone Propagation in the Northern Hemisphere to Global Warming. J. Climate, 36, 7123–7142, 2023, https://doi.org/10.1175/JCLI-D-23-0082.1.

Hersbach HB et al., Complete ERA5 from 1979, Fifth generation of ECMWF atmospheric reanalyses of the global climate. Copernicus Climate Change Service (C3S) Data Store (CDS), 2017 (Accessed on 01 Jul 2022).

Mizuta R, A. Murata, M. Ishii et al, Over 5,000 Years of Ensemble Future Climate Simulations by 60-km Global and 20-km Regional Atmospheric Models, Bull Am Meteorol Soc 98, 1383–1398, 2017.

Murray RJ., Simmonds I, A numerical scheme for tracking cyclone centres from digital data. Part I: Development and operation of the scheme. Aust. Met. Mag., 39, 155-166. 1991.

Tamarin T, Kaspi Y, The poleward shift of storm tracks under global warming: A Lagrangian perspective, Geophys. Res. Lett., 44, 10,666–10,674, 2017, doi:10.1002/2017GL073633.

OMo8

Drivers of Near-Surface Wind Variability in the Denman Glacier Basin in East Antarctica under the Modulation of Synoptic Forcing

Zhaohui Wang[1,2], Laurie Menviel[1,2] Alex Sen Gupta[1,2,3], Zijian Chen[4], Thomas Caton Harrison[5], and Ian Goodwin[1,2]

[1]*Climate Change Research Centre, University of New South Wales, Sydney, Australia*
[2]*ARC Australian Centre for Excellence in Antarctic Science, University of New South Wales, Sydney, Australia*
[3]*Australian Research Council Centre of Excellence for Climate Extremes, Sydney, Australia*
[4]*School of Atmospheric Sciences, Sun Yat-sen University, Zhuhai, China*
[5]*British Antarctic Survey, Cambridge, United Kingdom*

Denman Glacier Basin, a critical region for studying polar ice dynamics and climate change impacts, is heavily influenced by the combination of topographic and atmospheric conditions, particularly experiencing strong downslope winds. This study examines the structure and variability of near-surface winds in the basin, focusing on the influence of large-scale circulation, synoptic weathers, and local orographic effects. Through high-resolution atmospheric simulation experiments, we demonstrate the forced components of near-surface winds during three prevalent synoptic systems in the area, quantifying the relative contribution of large-scale and surface-driven forces in shaping wind structure and variability. We also conduct perturbation experiments with topographies of varying resolutions to examine the orographic controls on the spatial climatology of downslope winds, in response to a range of synoptic systems typical to the region. Our findings help clarify uncertainties in interpreting snow accumulation variability in ice cores and determining whether modern regional mass balance trends result from increased glacial discharge or shifts in synoptic circulation. The findings will be used to interpret the Denman Glacier discharge, snow accumulation over the basin, aiding in the interpretation of recent ice core data collected in the recent field season.

OMo9

Detection of Extremely Weak Precipitation at Two Antarctic Sites: Syowa Station and Dome Fuji

Naohiko Hirasawa[1,2], Yasushi Fujiyoshi[3], Koji Fujita[4], Masanori Yabuki[5], Hiroyuki Konishi[6], Katsushi Iwamoto[7]

[1]*National Institute of Polar Research*
[2]*Sokendai (The Graduate University for Advanced Studies)*
[3]*Emeritus Prof., Hokkaido University,*
[4]*Nagoya University,*
[5]*Research Institute for Sustainable Humanosphere, Kyoto University*
[6]*Osaka-Kyoiku University,*
[7]*Fisheries Research Division, City of Mombetsu, Hokkaido*

In Antarctica, annual precipitation amounts are extremely low and precipitation intensity is weak compared with other regions, due to the continent's generally low temperatures and resulting low atmospheric water vapor cintent. Even during relatively heavy events associated with synoptic-scale disturbances, daily precipitation typically ranges from several tens of millimeters in coastal areas to only a few millimeters in inland regions,

If approximately half of the annual precipitation is attributable to clear-sky precipitation and occurs over 180 days (half the year), the corresponding mean daily rates are about 0.56 mm/day (0.02 mm/h) at Syowa Station and 0.08 mm/day (0.003 mm/h) in inland areas. These rates are below the resolution of the widely used Geonor T200B weighing gauge (≈0.04 mm), making it insufficient for measuring clear-sky precipitation on an hourly basis.

Lidars and laser disdrometers can detect very weak precipitation. For ice-particle precipitation, the laser backscattering intensity depends not only on the number of particles but also on crystal shape and face orientation. Hirasawa and Konishi (2025) [R1] demonstrated that a ceilometer and a disdrometer successfully detected extremely weak precipitation in Rikubetsu, northern Japan, one of the country's coldest regions.

The present study focuses on the detecting and quantitatively evaluating extremely weak precipitation at two Antarctic observation sites: Syowa Station and Dome Fuji. Syowa Station, located on the coast, experiences relatively higher precipitation rates for Antarctica, whereas Dome Fuji, situated on the inland plateau at an altitude of 3,800 m, experiences extremely weak precipitation. At Dome Fuji, clear-sky precipitation such as diamond dust occurs for a substantial portion of the year.

First, extremely weak precipitation at Syowa Station was investigated, with weighing gauge measurements used as reference data to calibrate precipitation intensities from a ceilometer and a laser disdrometer. The resulting relationship was then applied to ceilometer measurements at Dome Fuji. The presentation will discuss the results and their implications.

References

R1. Hirasawa and Konishi (2025): Okhotsk Sea and Polar Oceans Research, 9, 8-17. doi.org/10.57287/ospor.9.8

Interannual trend of precipitation at Dome Fuji station and indication of a potential impact from the South Atlantic Ocean

Kyohei Yamada[1], Jun Inoue[1,2], Naohiko Hirasawa[1,2], and Kazutoshi Sato[1,2]
[1]*National Institute of Polar Research*
[2]*Graduate University for Advanced Studies, SOKENDAI*

Although snowfall is one of the most important factors deciding surface mass balance over Antarctica, the knowledge of interannual trends in the region of the Antarctic interior is limited. From February 2003 to January 2004, the 44th Japanese Antarctic Research Expedition (JARE44) conducted year-long observations of surface climate, radiation budget, ceilometer backscatter profiles, and precipitation amount at Dome Fuji Station (DF; 77.32°S, 39.70°E; 3810 m a.s.l.). To analyze the long-term trend of precipitation at Dome Fuji in the Antarctic interior, we estimate 46 years of variations using reanalysis data corrected with the observational data.

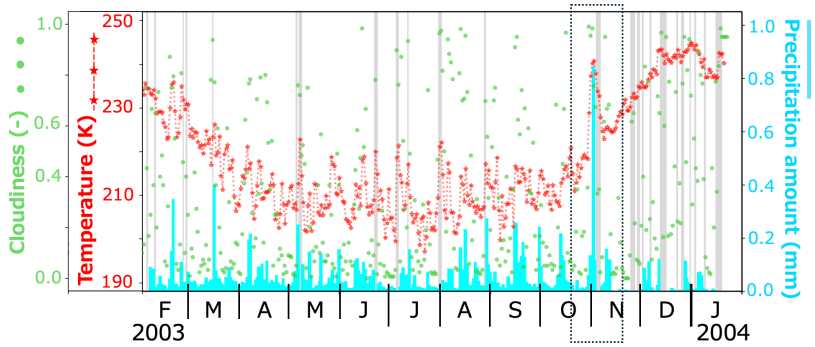

Figure 1. Observed surface air temperature (red), cloudiness (green), and precipitation amount (blue) at DF for JARE44 period. Gray lines indicate days excluded due to the potential for strong blowing snow.

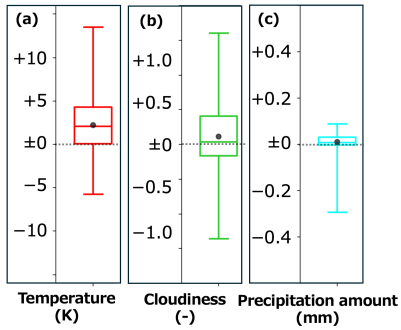

Figure 2. Differences of observed surface air temperature, cloudiness, and precipitation amount from ERA5 reanalysis for JARE44 period.

Figure 1 shows the observed surface air temperature, cloudiness, and precipitation. Since the sampling method (Fujita & Abe, 2006) may overestimate precipitation during strong blowing snow events, days with strong blowing snow, which are detected by a ceilometer, were excluded from the analysis. The box plots in Figure 2 indicate that ERA5 generally reproduces surface air temperature, cloudiness, and precipitation amount reasonably well. Surface air temperature exhibits a seasonal cycle with a “coreless winter,” fluctuating approximately between 205 and 245 K. During extreme precipitation events (EPEs), temperature occasionally increases rapidly alongside large precipitation and enhanced cloudiness. One such EPE occurred in early November 2003, when precipitation exceeded 1 mm over three days, accompanied by a temperature increase of approximately 20 K. During this event, a strong pressure ridge associated with a blocking high was observed (Figure 3). This blocking high caused an intrusion of warm, humid air into the Antarctic interior, leading to an increase of over 300% in the monthly mean integrated water vapor. Figure 4 illustrates surface air temperature, cloudiness, and precipitation during this EPE. ERA5 generally reproduced the in-situ observations; however, the diurnal cycle of surface air temperature in ERA5 was weaker than that observed. While the total precipitation amount during the event period was comparable between ERA5 and

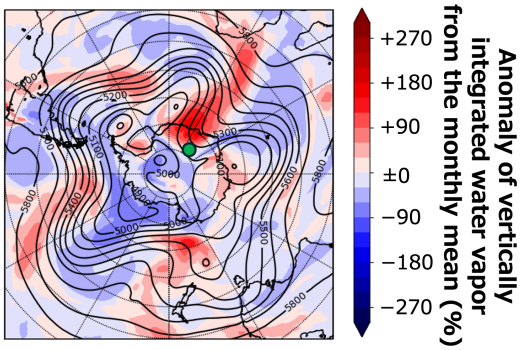

Figure 3. Anomaly of vertically integrated water vapor from the monthly mean (shade) and 500 hPa geopotential height (contour) on October 31st, 2003. Green circle is DF.

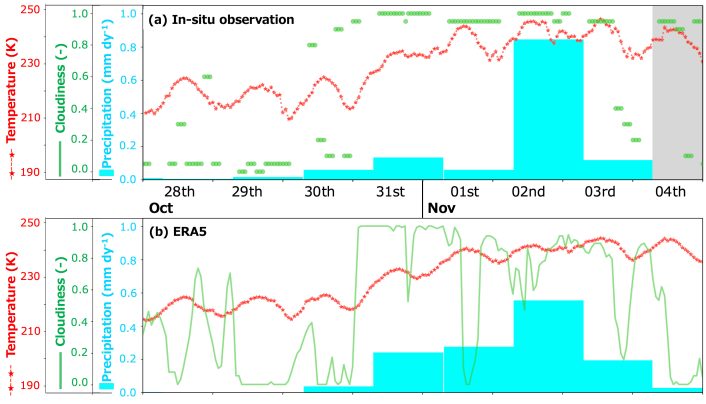

Figure 4. Surface air temperature, cloudiness, and precipitation amount of observation (upper) and ERA5 (lower) from October 28th to November 4th, 2003.

observations, ERA5 underestimated the peak precipitation and overestimated precipitation on the days before and after the peak. Therefore, precipitation comparisons were conducted using 3-day moving averages (Figure 5). During the JARE44 observation period, ERA5 underestimated precipitation by approximately 14%, with a correlation coefficient of 0.73. Hereafter, the precipitation data used for long-term analysis are corrected by a factor of 1.16 (i.e., 1/0.86).

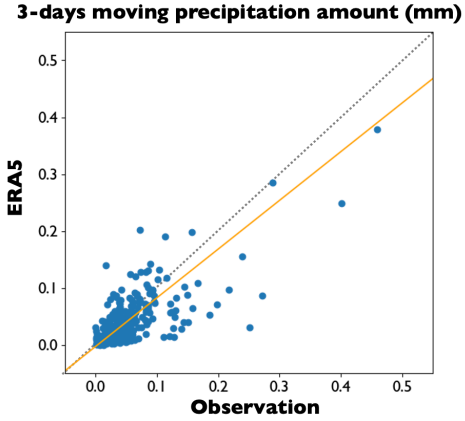

Figure 5. Scatter plots of 3-days moving precipitation amount for JARE44 period. Orange line is standardized major axis regression.

Figure 6 illustrates the time series of precipitation at DF for 46 years, from 1979 to 2024, in ERA5, corrected using observational data. The total precipitation shows an increasing trend of +0.11 mm/year, which is statistically significant at the 99% confidence level according to the Mann–Kendall trend test. The precipitation associated with EPEs, which are defined as days with precipitation amount larger than 0.29 mm (mean plus 2-sigma), also shows a statistically significant increasing trend at the 99% confidence level, with an increment of +0.09 mm/year. In contrast, non-EPE precipitation does not exhibit a statistically significant trend. Additionally, the number of EPE days shows a significant increasing trend of +0.20 days/year. These results indicate that the increasing trend in total precipitation at DF is primarily driven by the increase in EPEs.

Long-term components of the climate system, such as decadal-scale variations in sea surface temperature (SST), can influence atmospheric blocking patterns (e.g., Fei et al., 2002). Figure 7 shows the SST trend and the correlation between SST and precipitation at DF over the 46 years in ERA5. SST in the South Atlantic Ocean, particularly within the region 30°W–30°E, 40°–50°S (hereafter referred to as SST_{SAO}), exhibits a strong correlation with precipitation at DF. This finding is consistent with the results of Sodemann and Stohl (2009), who showed that the primary moisture source for the East Antarctic Plateau originates from around 40°–45°S. SST_{SAO} also displays a statistically significant increasing trend at the 99% confidence level. As shown in Figure 6, while SST_{SAO} does not exhibit a consistently strong correlation with DF precipitation year-round, it is associated with intensified precipitation periods, such as those observed in 2009 and 2011. It is plausible that moisture originating from this region is transported to DF via atmospheric rivers, leading to enhanced precipitation events over Dronning Maud Land.

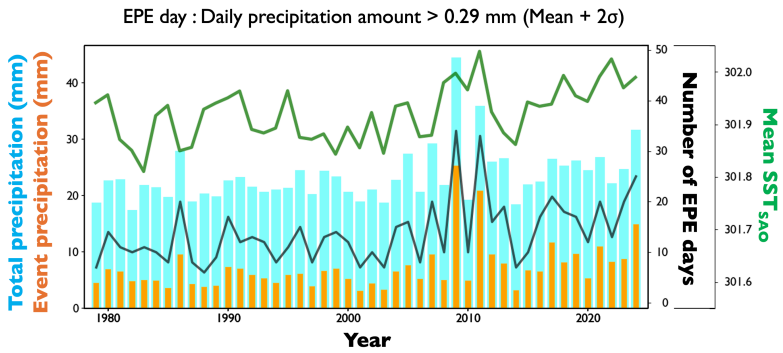

Figure 6. Time series of interannual changes of total precipitation amount (blue), EPE precipitation amount (orange), number of EPE days (black), and mean SSTSAO (green) for 46 years.

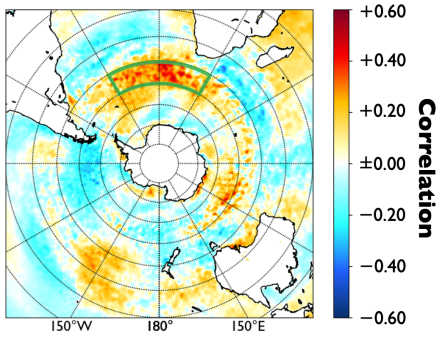

Figure 7. Correlation coefficient between precipitation amount at DF and sea surface temperature.

References

Fei, H., Faxiu, Z., & Xiaodan, Q. (2002). Interannual and decadal variability of the North Pacific blocking and its relationship to SST, teleconnection and storm tracks. Advances in Atmospheric Sciences, 19, 807-820.

Fujita, K. and O. Abe (2006): Stable isotopes in daily precipitation at Dome Fuji, East Antarctica. Geophys. Res. Lett., 33(18).

Hersbach, H., Bell, B., Berrisford, P., Hirahara, S., Horányi, A., Muñoz‐Sabater, J., ... & Thépaut, J. N. (2020). The ERA5 global reanalysis. Quarterly journal of the royal meteorological society, 146(730), 1999-2049.

Sodemann, H., & Stohl, A. (2009). Asymmetries in the moisture origin of Antarctic precipitation. Geophys. Res. Lett., 36(22).

OMo11

Early observation results of GOSAT-GW/AMSR3

Rigen Shimada[1], Misako Kachi[1], Eri Yoshizawa[1], Keiichi Ohara[1], Kentaro Aida[1], Kazuki Nakata[1], Takumi Suzuki[1], Takeshi Miura[2], Kazuya Inaoka[2], Yasushi Kojima[2] and Naoto Ebuchi[3]

[1]*Earth Observation Research Center, Japan Aerospace Exploration Agency*

[2]*GOSAT-GW Project Team, Japan Aerospace Exploration Agency*

[3]*Institute of Low Temperature Science, Hokkaido University*

The Global Observing SATellite for Greenhouse gases and Water cycle (GOSAT-GW), also known as "IBUKI GW," was successfully launched on June 29, 2025 (JST) and entered its nominal operational orbit on July 20. It carries two mission instruments: the Total Anthropogenic and Natural emissions mapping SpectrOmeter-3 (TANSO-3) and the Advanced Microwave Scanning Radiometer 3 (AMSR3). AMSR3, developed by JAXA, continues the legacy of AMSR-E and AMSR2 and began data acquisition on August 11 as part of its initial functional verification phase. AMSR3 observes naturally emitted and/or scattered microwaves from land, ocean, and atmosphere, enabling the estimation of geophysical parameters such as sea surface temperature, precipitation, and water vapor. It features 21 channels from 6.9 to 183 GHz, including five newly added channels: 10.3 GHz (V/H polarization), 165.5 GHz (V polarization), and 183.3±3/±7 GHz (V polarization). These high-frequency channels enhance sensitivity to ice particles, snowfall, and mid-to-upper atmospheric water vapor, improving detection of solid precipitation and cloud phase discrimination. Initial observations demonstrate AMSR3's capability to distinguish between rain and snow clouds, particularly in high-latitude regions. AMSR3 Brightness Temperature RGB composite image from August 15 to 17, 2025, reveals distinct cloud types: light purple areas indicating ice clouds and light green areas representing rain clouds (Figure 1). These observations are important for improving solid precipitation retrieval particularly in polar regions. AMSR3 is also expected to advance sea ice monitoring by building on AMSR series legacy. JAXA is currently conducting initial calibration and validation to ensure data quality, aiming to support global water cycle monitoring and cryospheric research. Version 1 of AMSR3 products will be released within one year of launch.

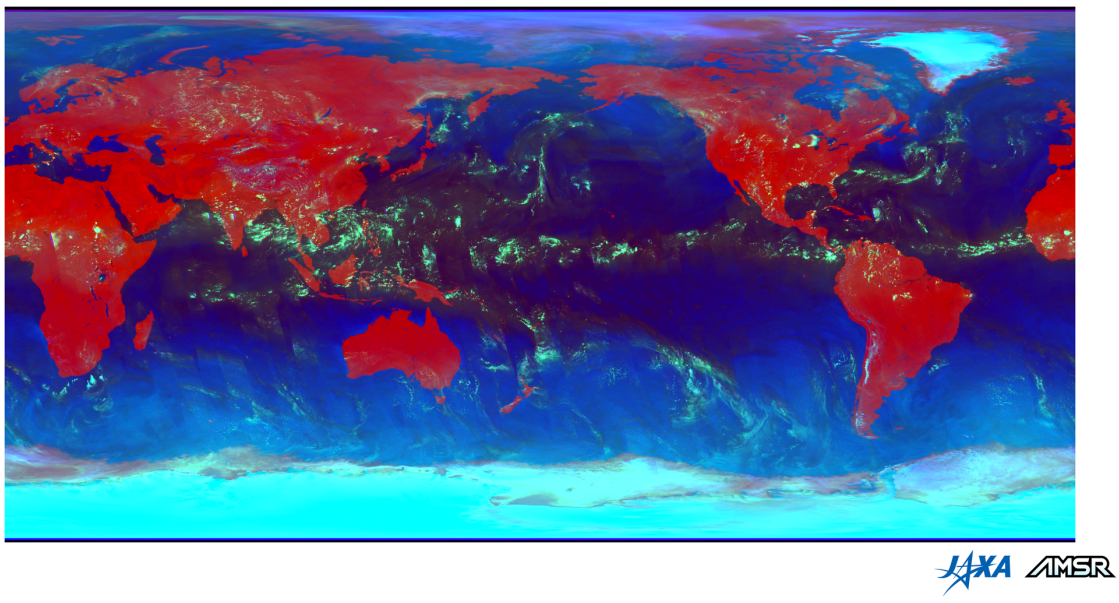

Figure 1. AMSR3 global observation image highlighting cloud and precipitation areas in light green (RGB composite image using 18.7, 89.0, and 165.5 GHz V-Pol. brightness temperature averaging data of ascending paths from August 15 to 17, 2025)

OMo12

Acoustic monitoring of proglacial discharge of Qaanaaq Glacier

Tomohiro M. Nakayama[1,3], Evgeny A. Podolskiy[1], Takuro Imazu[2,3], Kotaro Yazawa[2,3] and Shin Sugiyama[1,2]
[1]*Arctic Research Center, Hokkaido University,* [2]*Institute of Low Temperature Science, Hokkaido University,*
[3]*Graduate School of Environmental Science*

1. Background

Glaciers and ice caps along coastal Greenland have experienced significant mass loss in recent decades due to global warming (Hugonnet et al., 2021). This contributes not only to global sea level rise, but also to posing a serious threat of flood to local communities (Kondo et al., 2021). Therefore, continuous monitoring of proglacial discharge is crucial. However, conventional discharge monitoring methods cannot completely extract the discharge because its river channel and discharge rate change drastically. As an alternative, passive acoustic methods offer a cost and labor-efficient solution, allowing non-invasive monitoring by simply placing acoustic sensors near the stream (Osborne et al., 2021; Podolskiy et al., 2023). However, the advantages and limitations of this approach remain poorly understood.

2. Methods

In the summer of 2024, we deployed four acoustic sensors (Song Meter, Wildlife Acoustics) and two time-lapse cameras along the proglacial discharge of Qaanaaq Glacier, northwest Greenland (77.5 N, 69.0 W), to demonstrate the potential of comprehensive acoustic monitoring for discharge estimation (Figure1). We conducted repeated discharge measurements using an electromagnetic current meter 32 times, to establish a relationship between continuous water level measurements (recorded by a pressure sensor) and the acoustic data. Based on the water level–discharge curve, we reconstructed continuous discharge data from the water level measurements.

3. Results and Discussion

Our results demonstrate that the sound generated by the proglacial stream correlates with discharge at all stations and can serve as a continuous proxy for runoff. We divided the long-term spectrogram data into eight frequency bands and found that all sensors strongly correlated with discharge ($R \approx 0.90$) in the 94–375 Hz range, which is likely associated with the sound of flowing water. Additionally, we analyzed the time lag of the acoustic signal between the glacier terminus and a bridge located at 1800 m downstream. The time lag ranged from 36 to 48 minutes, and the flow velocity was estimated to be 0.65 m/s to 0.90 m/s, which was consistent with the observed value. Furthermore, we analyzed acoustic events recorded along the bridge over the proglacial stream to reveal the usage pattern of the road and bridge, as well as environmental activities near the river. As a result, we detected more than 400 acoustic events (e.g., traffic, construction machinery). This information could contribute to risk management efforts for stream flooding events.

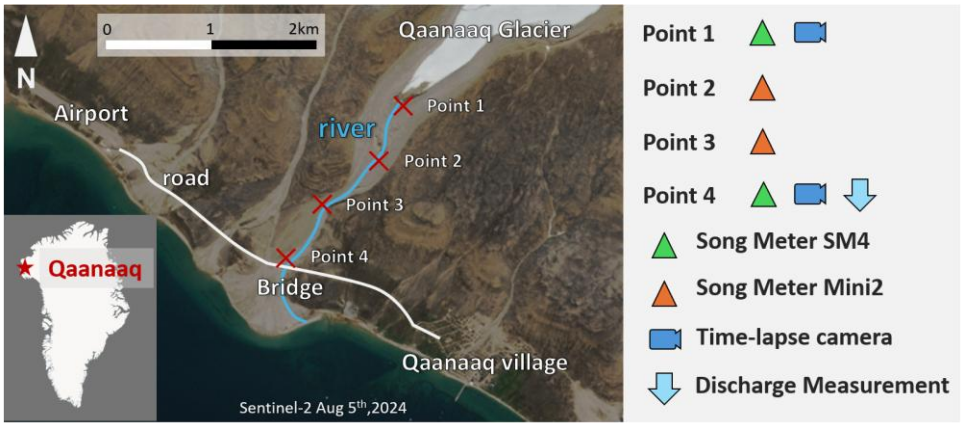

Figure 1. The distribution of all sensors (Song Meter SM4×2, Song Meter Mini2×2, time-lapse cameras×2) along the proglacial discharge of Qaanaaq glacier.

References

Hugonnet, R., McNabb, R., Berthier, E. *et al.* Accelerated global glacier mass loss in the early twenty-first century. *Nature* 592, 726–731 (2021). https://doi.org/10.1038/s41586-021-03436-z

Kondo K, Sugiyama S, Sakakibara D, Fukumoto S. Flood events caused by discharge from Qaanaaq Glacier, northwestern Greenland. *Journal of Glaciology*. 2021;67(263):500-510. https://doi.org/10.1017/jog.2021.3

Osborne, W.A., Hodge, R.A., Love, G.D., Hawkin, P. & Hawkin, R.E. (2021) Babbling brook to thunderous torrent: Using sound to monitor river stage. *Earth Surface Processes and Landforms*, 46(13), 2656–2670. Available from: https://doi.org/10.1002/esp.5199

Podolskiy, E. A., Imazu, T., & Sugiyama, S. (2023). Acoustic sensing of glacial discharge in Greenland. *Geophysical Research Letters*, 50, e2023GL103235. https://doi.org/10.1029/2023GL103235

OMo13

New ice-marginal lake inventory in Antarctica and its application for lake drainage detection

Shuntaro Hata[1], Moto Kawamata[2], Akihisa Hattori[1,3], Tsutomu Yamanokuchi[1], Kazuki Nakamura[4,] Yuichi Aoyama[1], Takanobu Sawagaki[5], and Jun'ichi Okuno[1,6]

[1]*National Institute of Polar Research*

[2]*Civil Engineering Research Institute for Cold Region, Public Works Research Institute*

[3]*Geography and Crustal Dynamics Research Center, Geospatial Information Authority of Japan*

[4]*College of Engineering, Nihon University*

[5]*Faculty of Social Sciences, Hosei University*

[6]*Joint Support-Center for Data Science Research, Research Organization of Information and Systems*

Ice-marginal lake forms in between rock outcrop region and glacial ice-bodies, i.e., ice sheets, ice shelves, and glaciers. GLOFs (glacial lake outburst floods) are the phenomenon of the abrupt and unexpected drainage from such lakes, which are one of the major concerns of mountain society. Only recent years, several studies reported GLOFs from ice-marignal lakes in East Antarctica, still remain poorly understands in the GLOFs in the region and the role of ice-marginal lakes in the surrounding environments. One of the major reasons is that our understanding in glacial lakes is quite limited especially for their geographical information i.e., number, location, and extent. A comprehensive dataset of ice-marginal lakes are required to understand current state of the lakes and its variation in this region. Here, we present a new ice-marginal lake inventory over Antarctica and its application for lake drainage detection by combining satellite remote sensing datasets.

Ice-marginal lakes were delineated by manual mapping for 18 regions over Antarctica. The mapping was processed based on visual inspection of the cloud-removed composite of Sentinel-2 images acquired in austral summer of 2017–2022. Among the studied 18 regions, 409 ice-marginal lakes were identified from 16 regions, and revealed that 89% of the ice-marginal lakes were located in East Antarctica. The total area was 493.0±1.0 km^2, which was substantially greater than the previous lake inventories.

The water drainage events of ice-marginal lakes were investigated by using REMA (Reference Elevation Model of Antarctica) version s2s041, which is a 2-m-resolution digital elevation models (DEMs) covering entire Antarctica. The REMA-strip DEMs including ice-marginal lakes were masked by using quality information included in each scene, and the masked DEMs were resampled to 100-m-resolution DEMs. The elevation differences relative to REMA-mosaic DEMs were utilized to detect water level change. Local concentration of surface lowering would be visualized in the elevation difference when an ice-marginal lake drained (Figure 1). From the elevation changes, drainage events were found from ten individual ice-marginal lakes in 2009–2024 period. The lakes also showed lake filling not only the drainage, which would have potential to understand the drinage mechanism, i.e., outburst via subglacial environments and whether they have cyclic drainage patterns as like ice-marginal lakes in other regions.

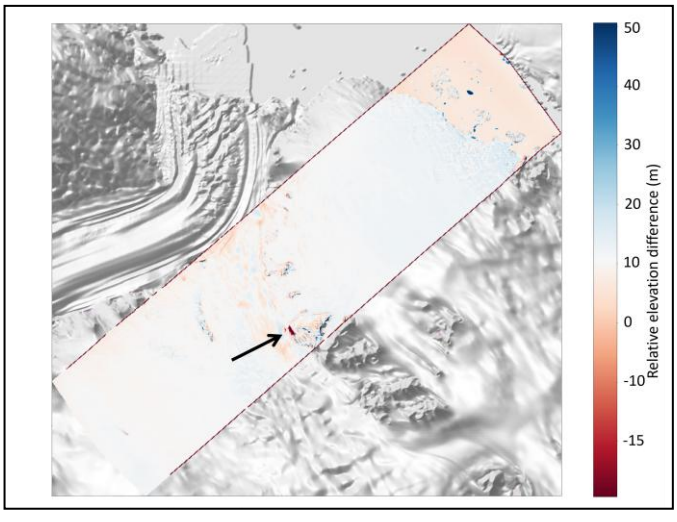

Figure 1. An example of elevation difference used for drainage detection. Black arrow indicates the ice-marginal lake that drained during the study period. Note that the elevation difference includes bias of REMA-strip, white color indicates the median elevation change between the REMA-strip and REMA-mosaic.

OMo14

Black Carbon Effects and Ion–Trace-Element Sources in the Godwin-Austen Glacier Snowpack

Nicolás González-Santacruz[1], Francisco Fernandoy[2], Jorge Pey[3], Kumiko Goto-Azuma[4], Motohiro Hirabayashi[4], Jon Arrizabalaga-Iriarte[1,5], Raúl R. Cordero[6], Sarah Feron[6,7], and Sérgio Henrique Faria[1,8]

[1]*Basque Centre for Climate Change (BC3), Leioa, Spain*
[2]*Laboratorio de Análisis Isotópico, Universidad Andrés Bello, Viña del Mar, Chile*
[3]*Instituto Pirenaico de Ecología (IPE), Zaragoza, Spain*
[4] *National Institute of Polar Research (NIPR), Tachikawa, Tokyo, Japan*
[5]*Faculty of Science and Technology, University of the Basque Country (UPV/EHU), Leioa, Spain*
[6]*Universidad de Santiago de Chile, Santiago, Chile*
[7]*University of Groningen, Leeuwarden, The Netherlands*
[8]*IKERBASQUE, Basque Foundation for Science, Bilbao, Spain*

High Mountain Asia (HMA) is considered the Earth's "Third Pole" as it contains more snow and ice than any other region outside the poles. HMA plays a critical role in global atmospheric circulation and sustains freshwater resources for over two billion people. Unfortunately, it is showing clear signs of degradation with local warming rates nearly twice the global average. While often examined in regional contexts, its vast snow and ice volume and marked environmental sensitivity make it essential to global cryosphere research. However, long-term in situ observations remain limited due to logistical difficulties and regional geopolitical constraints. Investigating the evolution of the HMA cryosphere provides valuable insights into the mechanisms driving snow and ice loss and highlights its significance for understanding cryosphere–climate interactions at low latitudes.

Here we present two case studies from the Central Karakoram Range (western HMA), both based on data collected from two snow pits excavated during the winter of 2018–2019 on the Godwin-Austen Glacier, complemented by samples from K2 high-altitude camps. The first quantifies black carbon concentrations in the snowpack and examines how these carbon-rich particles reduce albedo and accelerate melt dynamics. The second investigates the distribution of major ions (e.g., Ca^{2+}, Mg^{2+}, SO_4^{2-}) and trace elements (e.g., Sr, Ba, Li), assessing their seasonal variations and the relative contributions of crustal and anthropogenic sources. The studies employ stable isotope analysis, ion chromatography for major ions, inductively coupled plasma mass spectrometry (ICP–MS) for trace elements, single-particle soot photometry (SP2) for black carbon, and atmospheric back-trajectory modeling. Together, these studies illustrate the vulnerability of the HMA cryosphere to both regional and large-scale drivers, while offering complementary perspectives for polar research into cryosphere–climate interactions.

OMo15

Automated extraction of ice and firn microstructural features via image processing

Jon Arrizabalaga-Iriarte[1,2], Nicolás González-Santacruz[1], Sérgio Henrique Faria[1,3]

[1]*Basque Centre for Climate Change (BC3). Leioa, Spain*
[2]*Faculty of Science and Technology, University of the Basque Country (UPV/EHU). Leioa, Spain*
[3]*IKERBASQUE, Basque Foundation for Science. Bilbao, Spain*

Not only does the cryosphere play a critical role in climate, sea level, and water availability, among others, but ice also provides one of the most detailed records of our past climates. This information is stored in multiple proxies within the ice composition and microstructure, and it can be inferred from meticulous measurements and analyses. However, the correct interpretation of these records strongly depends on a proper understanding of the formation and evolution of the climate proxies, which makes the study of the involved microscopic processes crucial for this purpose.

Ice microstructure can be visually examined by characterizing sublimation-etched samples under an optical microscope. This technique, called Microstructure Mapping, has already provided many insights into these microscopic processes that control the behaviour of ice. Unfortunately, the expert inspection of ice micrographs is a time-consuming and labor-intensive process that results in most samples only being partially analyzed. It was soon recognized that any attempt at extracting the most information would require the automation of this mapping. This sparked an interest in developing new analysis tools that have so far worked well in specific applications but usually still require heavy manual validation and postprocessing.

Here, we present a new image processing tool that aims at automatically characterizing a broad range of microstructural features of an ice or firn sample. Currently, the program satisfactorily detects grains, subgrains, bubbles, pores, and triple junctions, after which different morphometric analyses are performed on the segmentation masks. This is accomplished with a combination of image processing operations (i.e., erode, dilate, morphological openings, closings, thresholdings, and other global and local metrics) and connected component analyses. Reducing the computational cost and the validation and postprocessing workload has been a priority to ensure the scalability to bigger projects. Additionally, we have implemented customization and extension options to cover as many applications as possible. This approach offers a versatile tool for large ice-core projects that streamlines the microstructural characterization of micrographs while aiming at optimizing the segmentation accuracy.

OMo16

Non-dimensional forms of basal sliding laws and flow laws for ice-sheet and glacier modelling

Ralf Greve[1,2]
[1]*Institute of Low Temperature Science, Hokkaido University, Sapporo, Japan*
[2]*Arctic Research Center, Hokkaido University, Sapporo, Japan*

Ice sheets and glaciers flow through basal sliding and internal deformation, each governed by physical laws commonly expressed as power-law relationships. These formulations include multiplicative coefficients – the sliding coefficient and rate factor – whose values and units depend on the respective exponents. This dependency complicates the systematic exploration of parameter space, especially in ensemble simulations. To address this, we propose dimensionless formulations of both sliding and flow laws, in which the coefficients are of order unity and decoupled from the exponents. This separation simplifies sensitivity studies and parameter variations. The dimensionless laws are straightforward to implement in existing models; we demonstrate this with the SICOPOLIS ice-sheet model using three test simulations in an academic set-up (Fig. 1). These simulations illustrate that independent variation of exponents and coefficients is feasible and practical, supporting the use of dimensionless laws in efforts to better constrain ice dynamics in past and future climate scenarios.

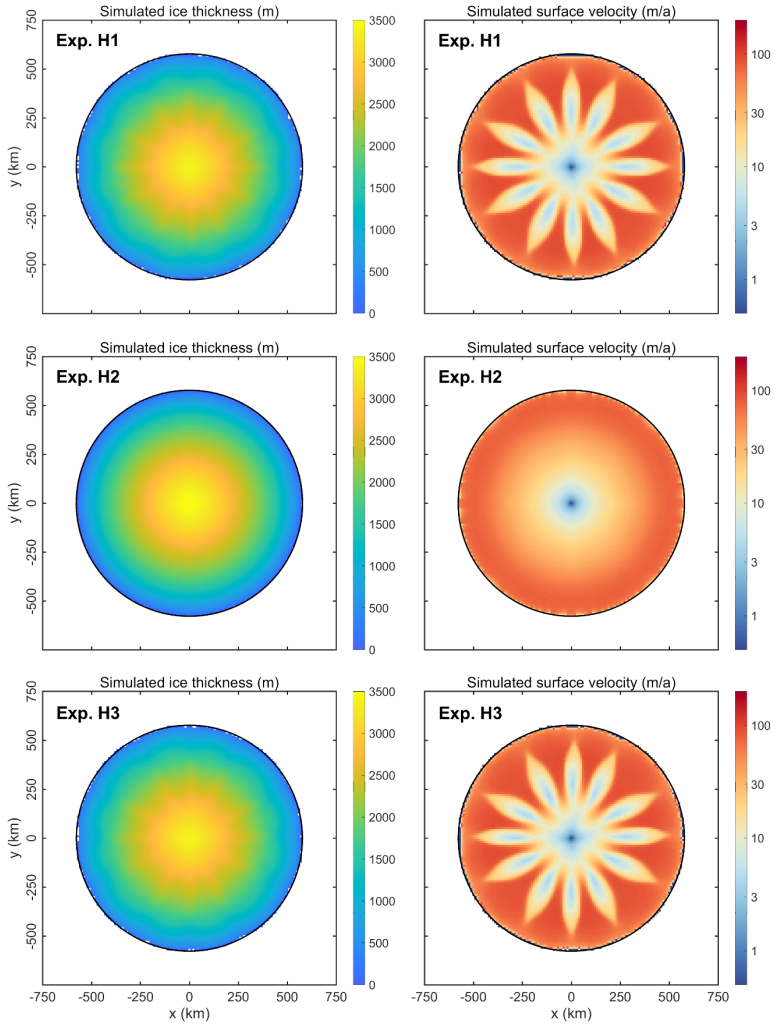

Figure 1. Simulated ice thickness and surface velocity for the three EISMINT-type experiments H1, H2, H3 after 100 ka model time. Exp. H1 is essentially Exp. H by Payne and others (2000): Weertman-Budd sliding law $v \sim \tau^p/N^q$ (v: basal sliding velocity, τ: basal shear stress, N: basal normal stress) with exponents $p = 1$, $q = 0$, Nye-Glen flow law with stress exponent $n = 3$. Change for Exp. H2: $p = 3$, $q = 2$; change for Exp. H3: $n = 4$. The same dimensionless sliding coefficient and rate factor have been used for the three experiments. For further details of the set-up, see Greve (2025).

The three experiments produce reasonable, nicely consistent results for the same dimensionless sliding coefficient and rate factor (both of order unity), even though the exponents in the sliding law and the flow law have been varied. In a dimensional formulation, this would not be possible because the changed exponents would require changes in the numerical values of the sliding coefficient and the rate factor by several orders of magnitude.

References

Greve R 2025. On non-dimensional forms of basal sliding laws and flow laws for ice-sheet and glacier modelling. Zenodo, doi: 10.5281/zenodo.15743001 (preprint).

Payne AJ and 10 others. 2000. Results from the EISMINT model intercomparison: the effects of thermomechanical coupling. Journal of Glaciology 46, 227–238, doi: 10.3189/172756500781832891.

OMp1

Methane concentration and its stable carbon isotopic ratios of late summer brash sea ice in the Pacific Sector of the Arctic Ocean

Ryuei Takeda[1], Daiki Nomura[1], Sohiko Kameyama[2], Manami Tozawa[3],
Amane Fuziwara[4], Yuri Fukai[4], Mariko Hatta[4], Masato Ito[5], Ryota Akino[1], Urumu Tsunogai[6]
[1]*Faculty of Fisheries Sciences, Hokkaido University.*
[2]*Faculty of Environmental Earth Science, Hokkaido University.* [3]*National Institute of PolarResearch.* [4]*Japan Agency for Marine-Earth Science and Technology (JAMSTEC).* [5]*Graduate School of Frontier Sciences, The University of Tokyo.*
[6]*Graduate School of Environmental Studies, Nagoya University.*

To investigate the mechanisms controlling the methane concentration in late-summer Arctic brash ice in the Chukchi Sea, we collected sea-ice samples during 2024 expedition (MR24-05c) using a wire mesh pallet cage on the R/V Mirai. Each sea-ice sample was melted in a gas-tight bag under dark, cool conditions (+4°C). Some of these samples were dirty ice. We measured physical and biogeochemical parameters including salinity, oxygen stable isotopic compositions, turbidity, chlorophyll-*a* concentrations, nutrients, methane concentration, and the stable carbon isotopic compositions of methane.
Because of the low solubility of methane in melted sea ice, part of the gas escaped into the gas-tight bag during the melting process. To account for this, we first calculated the gas-phase volume using the formula developed by Schwerdtfeger (1963) and Cox and Weeks (1983), which estimates the gas volume fraction in sea ice from its density. We then calculated the methane concentration according to Henry's law, using Henry's constant corrected for salinity and water temperature following Wiesenburg and Guinasso (1979).
The total estimated methane concentrations within the sea ice samples ranged from 5.8 to 43.2 nmol L–1 (mean ± standard deviation: 19.37 ± 11.69 nmol L–1), generally higher concentration than those of surface waters in the same season in 2021 (7.1 ± 4.9 nmol L–1). These results indicate that sea ice serves as a source of methane to seawater and atmosphere during melting.
The $\delta^{13}C$ values of methane ranged from –52.2 to –41.5‰. Methane of biological origin, such as that derived from sedimentary organic matter, typically has a δ13C value between –110‰ and –60‰ (Whiticar et al., 1986; Whiticar, 1999; Kvenvolden, 1993; Kastner et al., 1998). The relatively the ^{13}C signature observed in sea-ice methane is likely the result of isotopic fractionation during retention of methane within the sea ice.

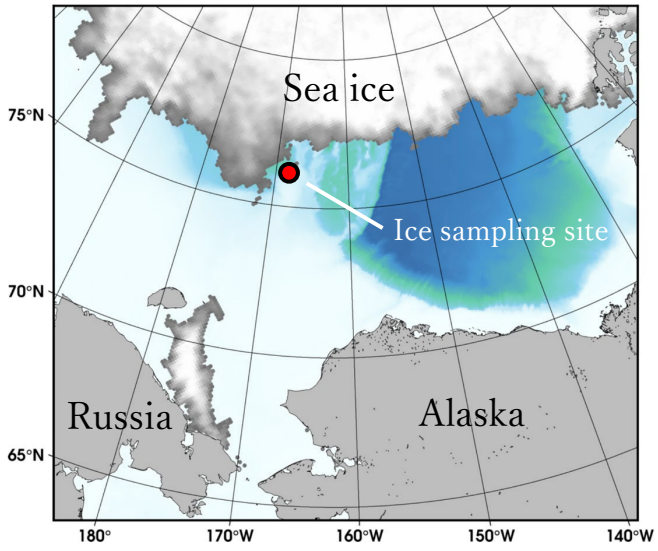

Fig. 1 Location where the floating ice samplings. were conducted. AMSR-2 sea ice concentration on Sep 17 is plotted with gray scale. (Quoted from R/V Mirai Cruise Report MR24-06C)

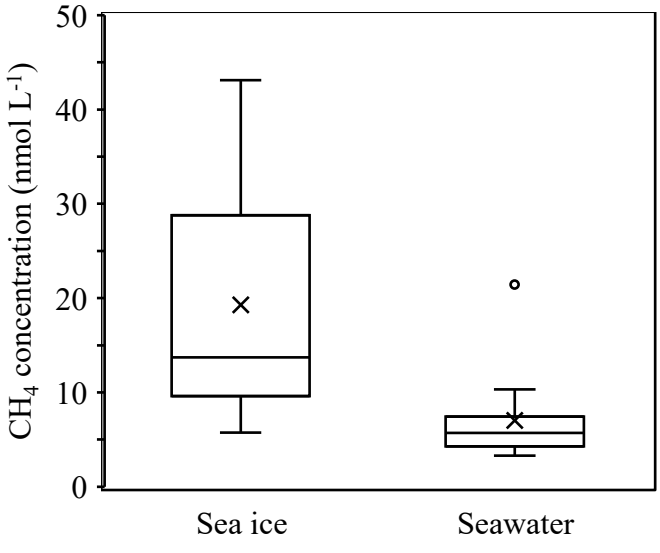

Fig. 2 Methene concentrations in sea ice and sea surface water in the same season.

References

Cox GFN, Weeks WF, Equations for Determining the Gas and Brine Volumes in Sea-Ice Samples. Journal of Glaciology. 29(102), 306-316, 1983

Kastner M et al., Chemistry, isotopic composition, and origin of a methane-hydrogen sulfide hydrate at the Cascadia subduction zone. Earth and Planetary Science Letters, 156(3-4), 173-183, 1998.
Kvenvolden KA, Gas hydrates—geological perspective and global change. Review of Geophysics, 31(2), 173-187, 1993.
R/V Mirai Cruise Report MR24-06C(MR24-Itoh) (URL: https://www.jamstec.go.jp/iace/e/report/pdf/MR24-06C_CruiseReport.pdf)
Schwerdtfeger P. The Thermal Properties of Sea Ice. *Journal of Glaciology*. 4(36), 789-807, 1963.
Whiticar MJ et al., Biogenic methane formation in marine and freshwater environments: CO_2 reduction *vs*. acetate fermentation—Isotope evidence. Geochimica et Cosmochimica Acta, 50(5), 693-709, 1986.
Whiticar MJ, Carbon and hydrogen isotope systematics of bacterial formation and oxidation of methane. Chemical Geology, 161(1-3), 291-314, 1999.
Wiesenburg DA and Guinasso Jr. NL, Equilibrium solubilities of methane, carbon monoxide, and hydrogen in water and sea water. J. Chem. Eng. Data, 24(4), 356–360, 1979.

OMp2

Estimation of sea ice thickness fluctuation using freezing degree days and snow depth in polar regions

Yoshifumi Harada[1] and Kazutaka Tateyama [2]
[1] *Graduate School of Engineering, Kitami Institute of Tecnology, Kitammi, Japan*
[2] *School of Earth, Energy and Environmental Engineering, Kitami Institute of Tecnology, Kitami, Japan*

Sea ice in polar regions plays an important role in the Earth's climate system and radiation balance. Observing both the distribution sea ice extent and sea ice thickness is essential for understanding the current state of climate change and predicting its future impact (Watanabe and Tateyama, 2021).

This study aims to visualize sea ice thickness fluctuation and focus on the increase of sea ice thickness driven by thermodynamic factors such as air temperature and snow depth. By comparing air temperature with sea ice thickness and snow depth with sea ice thickness, this analysis estimate sea ice thickness for days without observations. It clarifies the relationship between sea ice thickness and accumulated freezing degree days, as well as snow depth.

This analysis uses the longest available observed data series for sea ice thickness and snow depth from 1947 to 2024, provided by the Government of Canada through the Canadian Ice Thickness Program Collection, along with temperature reanalysis data from the ECMWF (the European Centre for Medium-Range). These locations are Alert (Alert LT1, Alert YLT), Eureka, Resolute, Cambridge Bay, Hall Beach, Coral Harbour, and Iqaluit, as shown in Figure 1.This analysis assumes a proportional relationship between freezing degree days and the ice thickness squared(Fukutomi et al., 1950). Figure 2 shows the relationship between freezing degree days and sea ice thickness squared at Eureka from 1947 to 2024 as an example. The red line indicates the change in sea ice thickness squared relative to freezing degree days. The figure shows that as freezing degree days increases, sea ice thickness squared increases sharply.Furthermore, their correlation coefficient was 0.94, indicating a strong correlation.

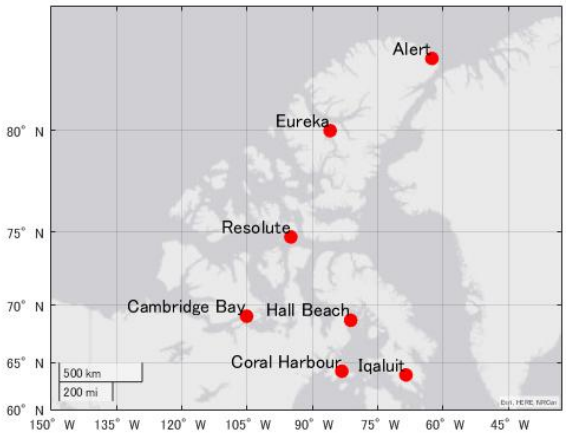

Figure 1. The observation points of sea ice thickness.

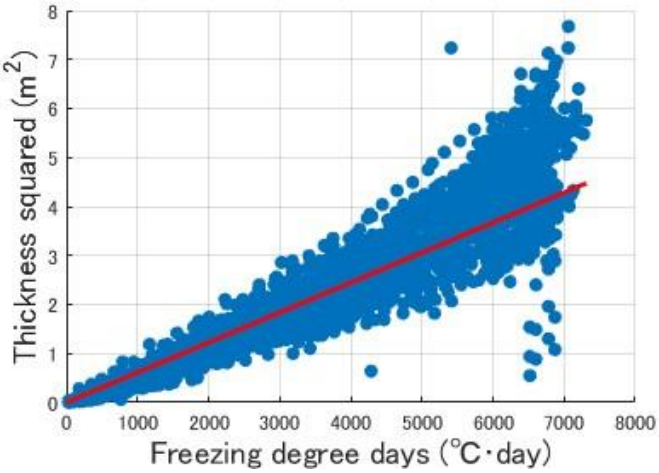

Figure 2. Relationship between sea ice thicness squared and freezing degree days at Eureka from 1947 to 2024

References

Tatsuya Watanabe and Kazutaka Tateyama(2021): An attempt to measure sea ice freeboard using UAV-SfM, Seppyo, 83(2), 155-167.

Takaharu Fukutomi, Koh Kusunoki and Tadashi Tabata(1950): Study of Sea-Ice (The 6th Report): On the Increase of the Thickness of Sea-Ice. Low Temperature Science, vol. 3, pp. 171–186. Hokkaido University.

OMp3

Development of an Algorithm for Mapping Sea Ice Topography in the Arctic Ocean Using Satellite L-Band SAR Images

Genta Ezawa[1,2], Takenobu Toyota[2] and Noriaki Kimura[3]
[1] *Graduate School of Environmental Science, Hokkaido University*
[2] *ILTS, Hokkaido University*
[3] *AORI, The University of Tokyo*

Recently in the Arctic Ocean, sea ice conditions have been changing rapidly, including a decline of sea ice extent, thinning of sea ice, an expansion of seasonal ice zone due to the decrease in multi-year ice (MYI) fraction. Associated with this, sea ice surface topography caused by deformation is also expected to be affected. While surface topography is important for estimating sea ice volume and predicting sea ice motion, observational data have been limited so far due to the lack of systematic measurements. To detect deformed ice area, past studies show that satellite L-band SAR is a useful tool (e.g. Toyota et al., 2021). However, due to the difficulty in validation, it has been difficult to convert SAR data to real topography. In this situtiation, ICESat-2, a satellite laser altimeter, was shown to be able to measure surface topography with good accuracy using an airborne laser profiler (Duncan and Farrel, 2022). Thus, the purpose of this study is to examine the validity of L-band SAR for detecting deformed ice, and develop an algorithm which converts SAR backscattering data (BS) to real deformed ice distribution, using ICESat-2 data.

For L-band SAR data, we used PALSAR-2 at a ScanSAR mode. Since SAR scattering data have a strong dependency on incidence angle, we investigated the incidence dependency for MYI in the Fram Strait beforehand, and used the HH signal normalized to the incidence angle of 40 degree. For sea ice height, ATL07 processing level data of ICESat-2 were used. The difference of observation time between these sensors was corrected using AMSR2-derived ice drift datasets with a resolution of 60 km. The analysis date is December 14, 2019 . To avoid discrepancy caused by local scale variations, we took a moving average of 500 m for comparison.

The result shows that these two datasets have a significant but not high correlation (r = 0.238). To improve it, we re-exmined the analysis by allowing for the error range of ice drift data (~0.2 cm/s) and seeking for the optimal correlation between these datasets. As a resultts, the correlation was improved up to r = 0.794, p<0.01 (Fig.1). Based on this result, we obtained the regression which converts BS to sail height and the surface roughness distribution is depicted in Fig.2 as an example. We intend to extend the result to other cases and examine the validity.

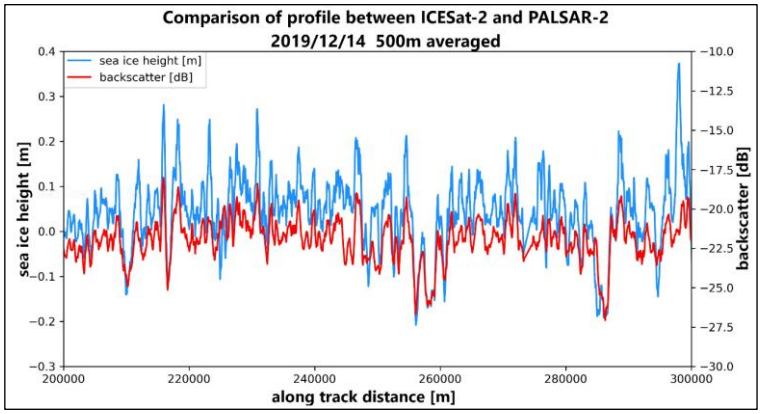

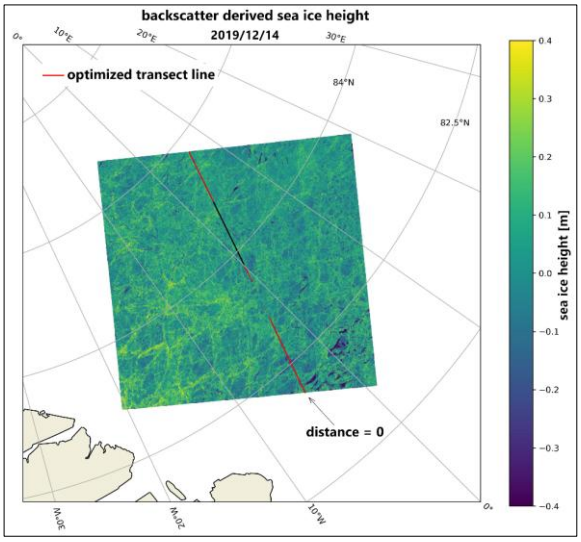

Figure1. Profile of sea ice height (blue) and backscatter of PALSAR-2 (red) (left)
Figure2. Sea ice topography map derived from backscatter (right)

References

Toyota et al., Measuring Deformed Sea Ice in Seasonal Ice Zones Using L-Band SAR Images. IEEE Transactions on Geosicience and Rremote Sensing, 59(11), 9361-9381, 2021.
Duncan and Farrell, Determining Variability in Arctic Sea Ice Pressure Ridge Topography With ICESat-2, Geophysical Research Letters, 49, e2022GL100272

OMp4

Relationship between total thickness and penetration distance during ramming of Shirase in Lützow-Holm Bay, East Antarctica

Shotaro Muraoka[1] and Kazutaka Tateyama[2]
[1]*Graduate School of Engineering, Kitami Institute of Technology, Kitami, Japan*
[2]*School of Earth, Energy and Environmental Engineering, Kitami Institute of Technology*

Since 2009, the 2nd generation Icebreaker AGB hereinafter referred to as Shirase has been the foundation of Antarctic observation, heading to Syowa Station in Lützow-Holm Bay every year. The Shirase can make continuous ice-breaking maneuvers depending on the ice conditions, and when navigating through areas of thicker, heavier multi-year ice, it can make intermittent ice-breaking maneuvers. Ramming is an ice-breaking operation that involves breaking through harsh ice-covered waters. It entails first retreating to establish an appropriate running up distance, then simultaneously applying the ship's kinetic energy and the thrust of the propulsion blades to accelerate the vessel. The bow is driven onto the ice, using the ship's momentum and weight to break through the ice. This process is repeated to gradually carve out a passage. The Shirase also performs various onboard observations before/after reaching Syowa Station, and one of the most important observations is the sea ice observation conducted when the ship enters the sea ice area. JARE has been conducting total thickness observations using an electromagnetic induction device (EM) on board the Shirase since the 42nd summer expedition in 2000 and has continued these observations to the present day. Total thickness is considered a factor contributing to the difficulty in navigation, , and the long ramming penetration distance indicates that the ice-breaking navigation was relatively ease. This is thought to reflect relatively small ice thickness and snow depth. The objective of this study is to compile a correlation diagram showing the relationship between the penetration distance achieved during the Shirase's ramming operations and total thickness at that time, thereby evaluating the navigational difficulty faced by the Shirase due to total thickness. Figure 1 shows the Shirase's route and sea ice concentration. To visualize sea ice information from sea ice concentration in Lützow-Holm Bay, we used satellite data from the Advanced Microwave Scanning Radiometer 2 (AMSR2) onboard the GCOM-W satellite to observe changes in water circulation. The green line indicates drift ice zone, and the red line indicates fast ice zone. The analysis area covers the Lützow-Holm Bay (35-45°E, 65-70°S). Figure 2 shows a correlation diagram of total thickness and penetration distance for 2022. The approximation curve is $y = 260.4896/x - 16.7241$, indicating a tendency for longer penetration distance with thinner total thickness. A characteristic feature is the dense clustering of plots below the approximation curve and the sparse distribution of plots above it. The densely clustered area likely indicates higher ramming counts and more severe ice conditions.

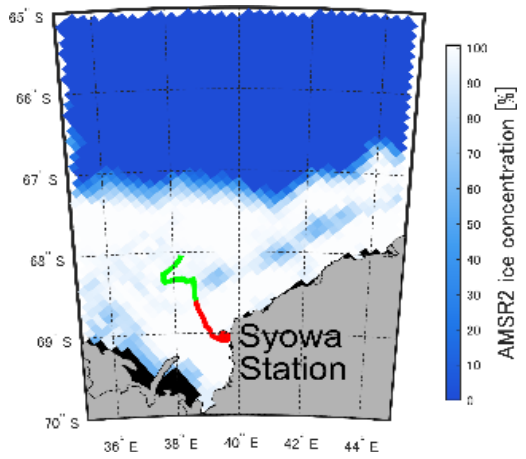

Figure1 Shirase's route and sea ice concentration

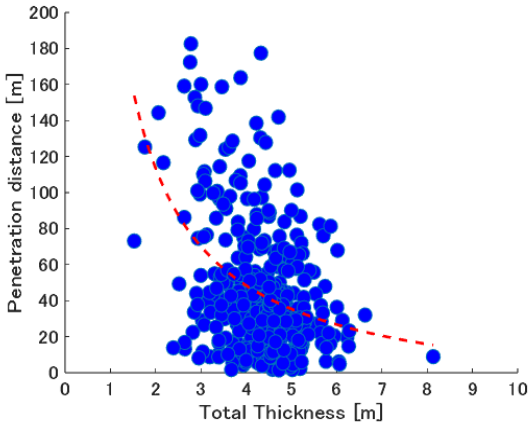

Figure2 Correlation between total thickness and penetration distance

Reference

Shigehara, S (2010): Icebreaker Operations Icebreaking Operations in the Ice Sea off Showa Station, 45, 186-191.
Ushio, S (2003): Frequent sea-ice breakup in Lutzow-Holmbukta, Antarctica, based on analysis of ice condition from 1980 to 2003, 47, 338-348.

Sea ice conditions in Lützow-Holm Bay, Antarctica, in 2025 : Unprecedented icescape in Ongul Strait

Shuki USHIO[1, 2]
[1]*National Institute of Polar Research*
[2]*The Graduate University for Advanced Studies, SOKENDAI*

To clarify sea ice distribution and its fluctuation factors in the Antarctic coastal regions, we have been continued sea ice monitoring using satellite imagery and meteorological/tidal data. This ice monitoring focuses particularly on landfast sea ice in Lützow-Holm Bay (LHB), where Syowa Station is located, and its surrounding areas. In-situ ice surveys have been conducted in coordination with the overwintering team. Furthermore, ice information obtained through the monitoring and previous findings are also crucial in supporting the navigation of the icebreaker Shirase, which accesses the station every summer.

In 2025, an extraordinary sea ice condition occurred in the Ongul Strait off the east coast of LHB, which appears to be unprecedented. This peculiarity is that the widespread breakup of the LHB landfast ice has led to the drifting of broken ice floes near Syowa Station, resulting in the formation of very close pack ice zone. As of early September 2025, the close pack-ice are expected to be severe enough to make navigation difficult for the Shirase. This presentation provides a preliminary report on the characteristics of sea ice conditions in 2025 and also reports on the ice history in LHB over the past 46 years.

The formation of this unusual sea ice condition has been observed in synthetic aperture radar satellite imagery late in April and confirmed by reports from the wintering team, as well as through visual observation from Syowa and drone aerial photography. In the close pack-ice zone, broken multi-year ice floes and icebergs are also frozen in place, with some areas of stacked floes reaching heights exceeding 3 meters. At present, it is difficult for us to predict if the ice in this sea area will remain frozen for an extended period or if it will suddenly undergo breakup. While attempting to analyze past cases of ice condition changes, we will continue ice monitoring, tracking not only changes occurring near the target sea area but also changes observed across the broader LHB region. Furthermore, ice monitoring will continue to assess the relationship between the sea ice extent in the offshore pack ice area and the ice conditions within the bay, together with meteorological conditions.

The information used in this presentation has been obtained with the cooperation of the JARE-66 wintering team and Center for Antarctic Programs.

OMp6

Analysis of absolute dynamic topography in the Australia-Antarctic Basin

Yuumi Hirayama[1], Yujiro Kitade[1]
[1]*Tokyo University of Marine Science and Technology*

The Australia-Antarctic Basin, located in the Indian Ocean sector of the Southern Ocean, is an important ocean region that is part of the pathway for the deep ocean circulation. In order to understand how global warming will affect the deep ocean circulation, it is necessary to clarify how the effects of weakened bottom water subduction occurring at the Antarctic margin will spread to lower latitudes and how transformed water masses will be incorporated into the global circulation. To date, no clear structure indicative of the circulation throughout the entire basin has been observed in the Australia-Antarctic Basin, and the mechanism governing material circulation in this region remains unknown. Therefore, we analyzed absolute dynamic topography data, which is continue in time and space, to investigate the characteristics of this region.

The analyzed data is CMEMS Absolute Dynamic Topography (ADT) grid data with a spatial resolution of 0.25° and a temporal resolution of 24 hours, covering 29 years from 1993 to 2021. Hovmöller diagrams of the ADT along the latitude showed a westward shift of the displacement from 135°E to 110°E. However, the temporal variation, magnitude, and east-west spacing of the displacement were not always constant, but rather varied in complex ways over time. Therefore, we performed a time-domain spectral analysis on all ADT data points, and for several periodic bands where clear peaks were observed, we calculated the frequency-integrated values of the power spectrum and examined the characteristics of its distribution. The values calculated here can be considered proportional to the available potential energy in each periodic band, and henceforth they will be referred to simply as the energy of each periodic band.

In the energy distribution of any periodic band, the energy in the northeast of the Kerguelen Plateau and in the shallow waters around 150°E located East of the Australia-Antarctic Basin, where currents is strong, was high. Some ocean regions showed significant differences depending on the periodic band. For example, Figure 1 shows the spatial distribution of the energy distribution for the 20-30 day and 50-60 day periodic bands. In the 20-30 day and 30-40 day periodic bands, high energy areas (areas surrounded by ellipses in the left of Figure 1) were observed near 60°S, along the contour lines of the Antarctic coast from 110°E to 135°E. Examining the temporal variations in these periodic bands, it was also confirmed that the variations propagated from east to west. Meanwhile, in the 50-60 day periodic band, high energy (indicated by arrows in the right of Figure1) was also observed in the area extending from 115°E to 135°E toward the deepest part of the basin (around 58°S), but this was not observed in the 20-30 day periodic band. Variations in this 50-60 day periodic band were confirmed to move west-northwest from around 140°E to 125°E.

Additionally, in the area of strong variations between 110°E and 135°E around 60°S, energy is especially high around 60°S ,110°E on a 20-30 day periodic band. This is thought to be a variation related to the approximately 20 day cycle observed in mooring observations offshore Vincenes Bay (107°E to 105°E at 64°S).

At the time of presentation, we will provide a more detailed report on the distribution of currents and their movement associated with each displacement.

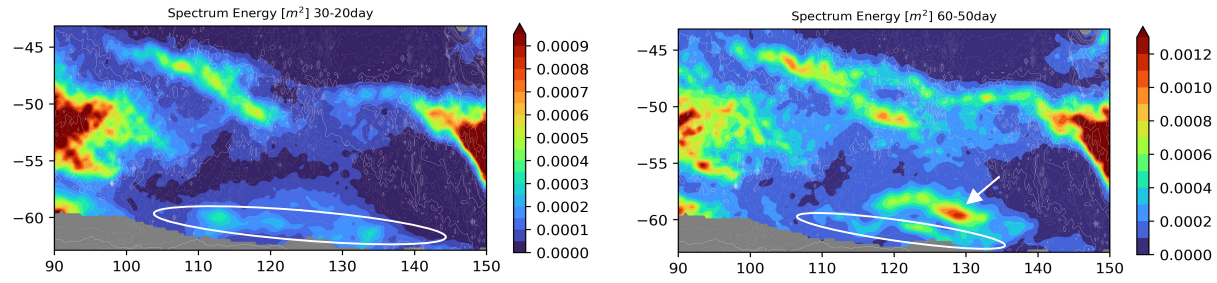

Figure 1. The spatial distribution of the dispersion of each periodic band (index of energy).
Left figure) 20-30day periodic band. Right figure) 50-60day periodic band.

OMp7

Water mass structure in the interior of the Indian Sector of the Southern Ocean

Juna Akamine[1], Yujiro Kitade[1]
[1]*Tokyo University of Marine Science and Technology*

Antarctic Bottom Water (AABW) formed by sea ice production and cooling in the coastal regions has been experiencing freshening and density decrease in recent years due to accelerated melting of glaciers and ice sheets caused by global warming. The warming observed in the bottom layer of the Southern Ocean suggests a weakening of the sinking of cold bottom water, the global heat and material transported by meridional overturning circulation is in danger of being weakened. Keishi Shimada et al. (2022) pointed out that the long-term freshening of the source waters of the AABW has reduced density, preventing the water from sinking to the abyssal layers and instead spreading northward along the neutral-density surface γn = 28.19. However, few studies have focused on the transformation of water masses and their spatial extent of the water mass with reduced density in the shallower layers. To understand the spread of the AABW that cannot sink (light AABW) in the shallower layers, spatially extensive data analysis is required. In this study, to clarify the spatial structure of the water masses in the intermediate and deep layers, we analyzed a wide range of the regions using Argo float data, instead of the previously used data observed along the line.

In this analysis, after applying quality control tuned to Southern Ocean water-mass characteristics to Argo data over the South Australian Basin and the Australian–Antarctic Basin (80–150° E, 40–70° S), we constructed and utilized a 1°×1° latitude-longitude gridded dataset. From the averaged water mass distribution for 2003 to 2023, the northward extension of cold water was observed in regions such as near Kerguelen at 80°E and around 150°E, where the ridges extend close to the Antarctic continent, as well as in a broad area between 100-120°E. These northward extensions likely mark regions where cold waters from the Antarctic margin are transported northward. Given that water masses are generally thought to spread along isopycnal surfaces, we first examined the distribution of water mass on γn = 28.19 isopycnal surface, as highlighted by Keishi Shimada et al. (2022). On this isopycnal surface, water-mass properties are nearly uniform and local contrasts are indistinct. However, in areas where cold water spreads northward, the isopycnals showed a raised structure. At fixed depths, these cold-water areas are slightly fresher and denser. These indicate wide range doming of isopycnals surface in near center of the basin and suggest the production of a baroclinic geostrophic flow current field.

These results imply that the observed cold water mass spreads horizontally rather than along isopycnal surface. In this region, the central ridge is interrupted and the seafloor topography is deepened steeply. The effect of the change in ACC flow paths and topography is thought to have formed an upwelling area and local circulation surrounding the upwelling area that results in material transport equatorward. The water mass with reduced density may be directly carried equatorward by this circulation. In the presentation we will also address TS characteristics and interannual variability of the distributions of water mass.

References

Keishi Shimada, Yujiro Kitade, Shigeru Aoki, Kohei Mizobata, LingqiaoCheng, Kunio T.Takahashi, Ryosuke Makabe, Jota Kanda & Tsuneo Odate(2022):Shoaling of abyssal ventilation in the Eastern Indian Sector of the Southern Ocean.
https://doi.org/10.1038/s43247-022-00445-2

OMp8

Emission of sea-salt aerosols from snow on sea-ice observed by Aerosol Chamber Experiments in polar region

K. Hara[1], T. Kuramoto[2], M. Matsumoto[3], S. Nishino[3], Y. Kurosaki[3], T. Yamasaki[4], S. Matoba[3]

[1]*Fukuoka University, Japan*
[2]*Tokai University, Japan*
[3]*ILTS, Hokkaido University, Japan*
[4]*AVANGNAG, Japan*

Sea-salt aerosols (SSA) are one of major aerosol constituents in troposphere. SSA plays important roles as cloud condensation nuclei (CCN) and sources of reactive halogen species through heterogeneous reactions on SSA. In polar regions during winter and early spring, SSA can be released also from snow surface on sea-ice under strong wind conditions (e.g., Hara et al., 2020). In spite of large efforts in field campaign and by model studies, SSA emission from snow surface on sea-ice has still dearth of knowledge and a large uncertainty (e.g., Yang et al., 2019; Hara et al., 2017; Frey et al, 2020). The uncertainty may result from (1) misestimation of emission flux, i.e., number concentrations of SSA and blowing snow under strong winds conditions and (2) lack of knowledge on specific emission/formation processes of SSA. To elucidate SSA emission from sea-ice area under strong wind conditions, we attempted to measure aerosol number size distributions under the artificial strong wind conditions in polar region.

Aerosol chamber experiments (ACEs) were conducted to measure aerosol number size distributions under artificial blowing snow conditions. In ACEs, aerosol number size distributions were measured using a portable scanning mobility particle sizer (SMPS: D_p (diameter) = 10-250 nm) and a portable optical particle counter (OPC: D_p >0.3, >0.5, >0.7, >1.0, >2.0, >5.0 μm). ACEs were conducted in Siorapaluk, Greenland in February 2023 and Saloma Lake, Japan in February – March, 2024 and 2025.

During blower operation in ACEs, blowing snow appeared in the chamber. Aerosol number concentrations increased in the measured size ranges (Fig. 1). In addition to strong enhancement in the number concentrations in coarse mode, the number concentrations in sizes of 70-200 and ca. 20 nm increased during blower operations. This result strongly implies that aerosol number size distributions of sea-salt aerosols immediately after emission from snow surface by wind blowing had multi-modal structure, although mono-modal structure was assumed in model study. Multi-modal size distributions were obtained in the other ACEs in Saloma Lake and Siorapaluk, Greenland. From comparison of three field campaigns, emission of SSA showed temperature dependence. Lower emission rate of SSA was obtained under warmer conditions.

References

Frey et al., (2020) ***Atmos. Chem. Phys.***, doi: 10.5194/acp-20-2549-2020
Hara et al., (2017) ***Atmos. Chem. Phys.***, doi: 10.5194/acp-17-8577-2017
Hara et al. (2020) ***Environ Sci Process Impacts***, doi:10.1039/d0em00092b
Ranjithkumar et al. (2025) ***Elem. Sci. Anth.***, doi: 10.1525/elementa.2024.00006
Yang et al., (2019) ***Atmos. Chem. Phys.***, doi: 10.5194/acp-19-8407-2019

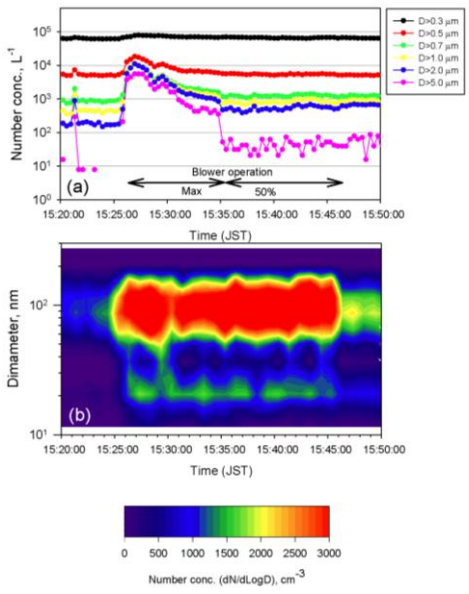

Figure 1. Short-term variations of (a) aerosol number concentrations measured by OPC and (b) aerosol size distributions measured by SMPS during ACEs in Saroma lake on 26 February 2024.

OMp9

Size distribution and chemical composition in size segragated aerosols in the Southern Ocean during the *Shirase* cruise of the 62nd/63rd Japanese Antractic Research Edition

Yayoi Inomata[1], Masataka Tsutsumi[2]. Keiichiro Hara[3], Naohiko Hirasawa[4], and Masahiko Hayashi[3]
[1]*Kanazawa University,* [2]*Kyusyu University,* [3]*Fukuoka University,* [4]*National Institute of Polar Research*

Atmospheric aerosol particles play important roles in the Earth's climate through the efficient scattering and absorption of solar radiation and cloud formation. The Southern Ocean is the southernmost ocean encircling Antarctica. Southern Ocean is far from the populated continental source, therefore, these region is an important to investigate spatiotemporal variation of natural aerosols. Under the strong and persistent westerly, sea salt particles are mechanically emitted and contribute dominant particulate mass in the marine boundary layer. In summer season, marine primary product is very active and high concentrations of gasous dimethyl sulfide (DMS) are observed. After emitted into the atmosphere, DMS is photooxidation and multiphase oxidation and yield to biogenic particle sulfur components, sulfate ($nssSO_4^{2-}$) and metane sulfonic acid (MSA). The aerosol partciles are act as cloud condensation nuclei (CCN) activity, which is strongly affected by chemical composition and particle size distribution. Emission of these natural aerosol and precursor gas are considered as an important part of the climate system. The purpose of this study is to investigate the particle size distribution and chemical composition of atmospheric aerosols in the Southern Ocean.

The observation of atmospheric aerosol particles over the Indian sector of Southern Ocean were conducted on the research vessel (R/V) *Shirase* during the 62nd and 63rd research cruises of the Japanese Antarctic Research Expedition (JARE). The size distribution of the ultrafine aerosol particles was measured using a scanning mobility particle sizing system (SMPS; Model 3085 for JARE62 and Model 3081 for JARE63, TSI Inc.). The size distribution was measured with the diameter for JARE62 being 4.5–156.8 nm and for JARE63 being 6.0–216.7 nm. The size distributions were scanned at 5-minute intervals. The concentrations of condensation nuclei (CN) were measured using a CPC (Model 3772) with a time resolution of one minute and averaged over five minutes for comparison with data obtained by SMPS. Additionally, aerosol particle measurements were performed using two types of optical particle counters (OPC): the KC22B (Rion Co., Ltd.; Dp > 0.08, > 0.1, > 0.2, > 0.3, and > 0.5 μm) and the KC-01D (Rion Co., Ltd.; Dp > 0.3, > 0.5, > 1, > 2, and > 5.0 μm). These aerosol particulate samples introduced into the measuring equipment through an intake port installed on the bow deck and a funnel was positioned at the stern deck. Data affected by ship exhaust emissions has been deleted. Data such as ship location information and meteorological conditions were measured as 10-second averages onboard. The data were calculated as 5-minute averages.

Figure 1 shows the horizontal distribution of CN concentration during the JARE62/63 along *Shirase* cruises. Areas exhibiting elevated concentrations were identified in the vicinity of the sea ice marginal zone.

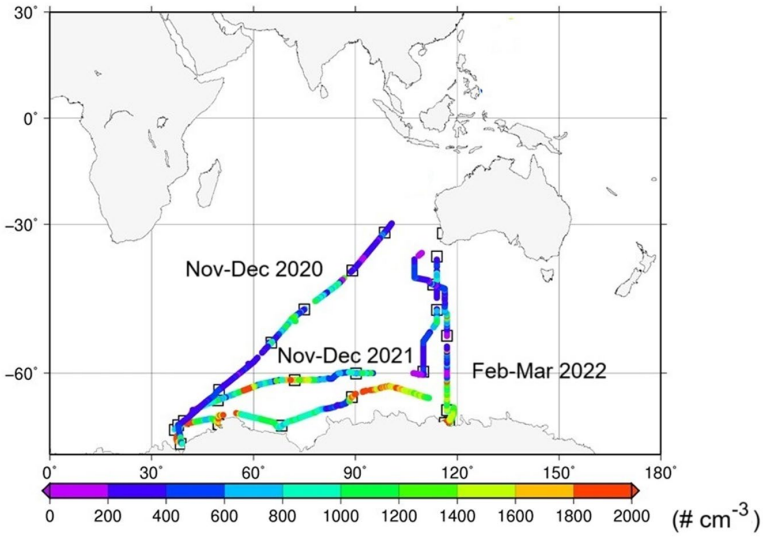

Figure 1. CN concentrations measured by CPC during the 2020/2021 and 2021/2022 Shirase cruises. Squares indicate the start points of filter sampling to measure chemical species.

Comparatively higher concentrations were also observed in the open ocean regions of the Southern Ocean (30–60°S). This finding suggests that new particle formation may occur not only at the sea ice marginal zone but also across a substantial oceanic region. The regions wherein higher concentrations were observed were not consistently associated with areas of high wind speeds or elevated chlorophyll fluorescence concentrations, which are indicators of biological activity.

The number size distribution of ultrafine particles, which were measured by SMPS and two OPC, during aerosol sampling periods for chemical analysis is approximated by lognormal distributions (Dal Maso et al., 2002). These existed in the forms of bi-modal, tri-modal, and quad-modal configurations. The diameter of the mode is distributed as follows: 3–6 nm for fresh nucleation, 11–29 nm for aged nucleation, 30–54 nm for the first Aitken, 77–101 nm for the second Aitken, and 102–211 nm for accumulation mode. Figure 2 shows the examples of number–size distributions of aerosol particles with quad-modal structure. In the region characterized by elevated CN concentrations and a marginal sea of ice, the size distribution of ultrafine particles tended to exhibit a higher number of modes. The relative contribution of fresh nucleation mode to total dN/dlogDp increased in the sea ice marginal zone.

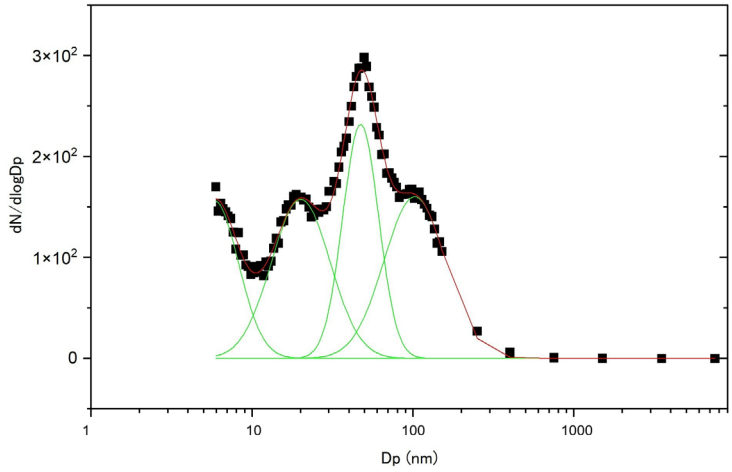

Figure 2. Number size distributions of ultrafine aerosol particles during aerosol sampling for chemical analysis. Black dots represent the measured mean particle size concentration distribution. Green lines represent calculated modes, while the red lines indicate the sum of fitted modes by curve fitting with log-normal distributions.

Atmospheric aerosols were collected during the *Shirase* cruises (JARE62 and JARE63) along the route between Fremantle and Showa Station. Samples were divided into six size classes with a 2–3 day time resolution (particle sizes $PM_{>10}$, $PM_{2.5–10}$, $PM_{1–2.5}$, $PM_{0.5–1}$, $PM_{0.1–0.5}$, $PM_{<0.1}$), and water-soluble ion concentrations were measured. Aerosols with a diameter smaller than 0.1 μm ($PM_{<0.1}$) are classified as ultrafine particles. In the case of JARE63, sea salt aerosols quantified through chemical analysis of aerosol filter samples were primarily present as coarse particles in the $PM_{1-2.5}$ (averaged 55% to total SSA) and $PM_{2.5-10}$ (averaged 25% to total SSA) fractions. Relative present of SSA in finer particles was estimated to be 8% for $PM_{0.5-1}$ and 4% for $PM_{0.1-0.5}$, and 3% for $PM_{<0.1}$. In contrast, $nssSO_4^{-2}$ and MSA were found to be abundant in the smaller particle. Size distribution of MSA was identified as larger particle sizes ($PM_{0.5-1}$ 51%; $PM_{1-2.5}$ 35%) than those of $nssSO_4^{2-}$ ($PM_{0.1-0.5}$ 26%; $PM_{0.5-1}$ 32%). These variations in the size distributions of $nssSO_4^{2-}$ and MSA may be indicative of differences in the formation and reaction processes occurring within the atmosphere. Concentrations of SSA, $nssSO_4^{2-}$, and MSA in $PM_{<0.1}$ (ultrafine aerosol particles), which are partially composed of CCN, amounted to 13.2–114.8 , 3.9–54.2, and ~8.1 ngm^{-3} for JARE63 in south of 60 °S, respectively.

References

Dal Maso, M, Kulmala M, Lehtinen KEJ, Mäkelä JM, Aalto P, O'Dowd CD, Condensation and coagulation sinks and formation of nucleation mode particles in coastal and boreal forest boundary layers. Journal of Geophysical Research: Atmospheres, 107(D19), 2002.

OMp10

Comparison of cloud fractions from Ceilometer and Micro-Pulse LIDAR observations around Syowa Station from JARE 55 to JARE 61

*Ayako Endo[1], Makoto Kuji[2], Masanori Yabuki[3] and Naohiko Hirasawa[4,5]
[1]*Graduate School of Humanities and Sciences, Nara Women's University*
[2]*Division of Natural Sciences, Faculty, Nara Women's University*
[3]*Research Institute for Sustainable Humanosphere, Kyoto University*
[4]*National Institute of Polar Research, Research Organization of Information and Systems*
[5]*Department of Polar Science, School of Multidisciplinary Sciences, SOKENDAI (The Graduate University for Advanced Studies)*

Cloud has opposite effects on the earth climate system: warming and cooling. Their magnitudes depend on cloud fraction, height, and so on. They influence the radiation balance on the earth and cloud is one of the greatest error sources for the climate prediction [IPCC, 2021]. Nevertheless, it is not easy to make a detailed observation due to their spatial and temporal variability. Furthermore, we do not have enough observation sites, especially over the ocean. It is also difficult to identify clouds using satellite images in polar regions because of the long polar nights and the similar optical characteristics between clouds and snow/ice [Yamanouchi, 2009]. Therefore, ground-based observations are necessary.

Cloud has been observed by different instruments onboard R/V *Shirase* and at Syowa Station in Antarctica. By comparing these observations, we can confirm the consistency of the analysis methods of previous studies. Furthermore, it will allow us to elucidate cloud behavior in detail. In this study, we investigated cloud fractions around Syowa Station based on the ceilometer and Micro-Pulse LIDAR observations.

Shipboard observations were carried out onboard R/V *Shirase* (AGB-5003) [Kuji et al., 2016]. The ceilometer (CL51, Vaisala) measures cloud base height with laser beams. The observation interval is 36 seconds. We analyzed 488,341 data sets during the berthing period around Syowa Station of the 55th to 61st Japanese Antarctic Research Expeditions (JARE 55 to JARE 61, i.e., from 2013 to 2020). Meanwhile, the Micro-Pulse LIDAR installed at Syowa Station observes at 1 min intervals. 103,244 data sets were analyzed during the berthing period of R/V *Shirase*. From these cloud base height data, the cloud fraction was evaluated as the frequency of occurrence.

As a result, it is found that the variation of the daily-averaged cloud fractions was generally consistent and the correlation coefficient was very high of 0.90.

Furthermore, we are going to compare the cloud fractions estimated from whole-sky camera observations during JARE 55 to 61 on the whole and discuss the characteristics of the cloud fractions around Syowa Station.

Acknowledgment

The shipborne observations were conducted in cooperation with Japan Aerospace Exploration Agency (JAXA) and National Institute of Polar Research. The authors are grateful to those who related to observations at Syowa Station and onboard R/V *Shirase* during JARE 55-61.

References

Hirasawa N., M. Yabuki, M. Shiobara, Y. Shimode and M. Kuji, Long-term all-sky-camera images and evaluated cloud-cover data at Syowa Station, Antarctica, Pol. Data Jour., 7, 35-49, 2023.

Intergovernmental Panel on Climate Change (IPCC2021), Climate Change 2021.

Kuji, M., R. Fujimoto, M. Miyagawa, R. Funada, M. Hori, H. Kobayashi, S. Koga, J. Matsushita, and M. Shiobara, Cloud fractions estimated from shipboard whole-sky camera and ceilometer observations, Transactions of the Japan Society for Aeronautical and Space Sciences, 14, 7-13, 2016.

Kuji, M., A. Murasaki, M. Hori, and M. Shiobara, Cloud Fractions Estimated from Shipboard Whole-sky Camera and Ceilometer Observations between East Asia and Antarctica. J. Meteor. Soc. Japan, 96, 201-214, 2018.

Yabuki, M., M. Shiobara, K. Nishinaka, and M. Kuji, Development of a cloud detection method from whole-sky color images, Polar Science, 8, 315-326, 2014.

Yamanouchi, T., Weather and Climate in Antarctic and Arctic, Tokyo: Seizando-Shoten, 2009 (in Japanese).

Yoshimura, M. and M. Yamashita, Contribution of Ground-Based Cloud Observation to Satellite-Based Cloud Discrimination, J. Environ. Sci. Eng. A, 2, 379-382, 2013.

OMp11

Toward Continuous High-Precision Precipitation Monitoring at Syowa Station, Antarctica

Naohiko Hirasawa[1,2], Madoka Oyama[3], Shuhei Kusano[3], Shohei Sato[3], Yusuke Kajiwara[3], Naoki Sakuramoto[3]

[1]*National Institute of Polar Research*
[2]*Sokendai (The Graduate University for Advanced Studies)*
[3]*Japan Meteorological Agency*

In its Strategic Plan (2024–2027), adopted at the 19th Session of the World Meteorological Organization (WMO) Congress in 2023, one of the priority areas is addressing the global and regional impacts of cryospheric change, including improved observations and research on future changes in the Antarctic ice sheet.

To contribute to this goal, the National Institute of Polar Research (NIPR) has operated four Automatic Weather Stations (AWSs) on the Antarctic ice sheet since 2017 under the Japanese Antarctic Research Expeditions (JARE), monitoring snow depth. From 2021 to 2022, precipitation amounts and formation processes were investigated at Syowa Station using a radar, a ceilometer, and a disdrometer (Hirasawa et al., 2022). However, at that time, continuous high-precision precipitation observations had not yet been planned. Trial measurements conducted by the Japan Meteorological Agency (JMA) during JARE-64 revealed that the resolution of commonly used rain gauges was insufficient to capture the weak precipitation intensities typical of polar regions and that they failed to record precipitation under strong wind conditions. These findings highlighted the need for improved measurement techniques and accurate assessment of the rain/snow ratio under climate warming.

This research aims to (1) establish continuous, high-precision precipitation monitoring at Syowa Station, (2) collect baseline data for automated rain/snow discrimination and classification of solid precipitation types, (3) investigate the relationship between wind speed and gauge catch ratio in snowfall conditions, and (4) develop techniques to distinguish heavy drifting snow from snowfall. Additional tests are being conducted to evaluate the performance of precipitation sensors during snow events.

These observations will contribute to the development of calibration data for radar-based measurements initiated in 2025. Data collected at Syowa Station—where solid and freezing precipitation occurs year-round—will help improve both measurement accuracy and classification methods. The outcomes are expected to support not only Antarctic research but also operational meteorological observations in Japan.

In this presentation, based on the observational results obtained so far, we discuss the currently most appropriate method and its observational accuracy for ground-based snowfall measurement at Syowa Station.

References

R1. Hirasawa et al. (2022): Okhotsk Sea and Polar Oceans Research, 6, 36-41. doi.org/10.57287/ospor.6.36

OMp12

Spatiotemporal distribution of correlation coefficients in wind patterns at NDF site and Syowa Station

Toshiki Kotake[1], Konosuke Sugiura[2], Masahiro Hori[2] and Naohiko Hirasawa[3]
[1]*Graduate School of Science and Engineering, University of Toyama*
[2]*Faculty of Sustainable Design, University of Toyama*
[3]*National Institute of Polar Research*

In recent years, rapid changes in the cryosphere have been progressing in polar regions due to rising temperatures. Understanding the actual state of the cryosphere is necessary because its impact on sea level rise is a concern. Wind speed and direction, which represent air movement in the atmosphere, are crucial for evaluating weather changes and heat exchange between the atmosphere and the snow and ice surface. Kotake et al. (2024) analyzed seasonal variations in wind speed and direction using 2022 data from an automatic weather station at NDF site in Antarctica and ERA-5 reanalysis data. The results indicated a slight predominance of northerly winds throughout the year. Furthermore, Kotake et al. (2025) examined the correlation between wind speeds at the NDF site and its surroundings in 2022. It was found that winds at the NDF site showed a high correlation throughout the year with winds originating from the west to southeast within a range of several hundred kilometers around part of the surrounding ice sheet summit. However, since this result is specific to 2022, this study aims to clarify the relationship between wind conditions at NDF stations and their surrounding areas over the past 30 years from 1993 to 2022, as well as to clarify the relationship between wind conditions at Syowa Station and its surrounding areas. To investigate the wind relationship between the NDF site and its surroundings historically, we used "ERA5 hourly data on single levels from 1940 to present". The correlation between hourly wind speeds at NDF locations and grid-based wind speeds was determined. Similarly, wind speed correlations were calculated for Syowa Station .

Over the past 30 years, the spatial distribution of correlation coefficients between NDF and surrounding areas, using NDF as the reference point in East Antarctica, showed high correlations throughout the year over a range of several hundred kilometers from the west to the southeast, consistent with the results from 2022 in Kotake et al. (2025) (figure omitted). Next, compared to the spatial distribution of correlation coefficients based on the 2022 NDF site in East Antarctica, Syowa Station showed higher correlations with the northern region, and the calculated correlation coefficients were both higher and lower in response to the coastal topography (Figure 1). Conversely, there was almost no correlation with the NDF site throughout the year. Both the NDF site and Syowa Station showed negative correlations with the eastern drainage basin.

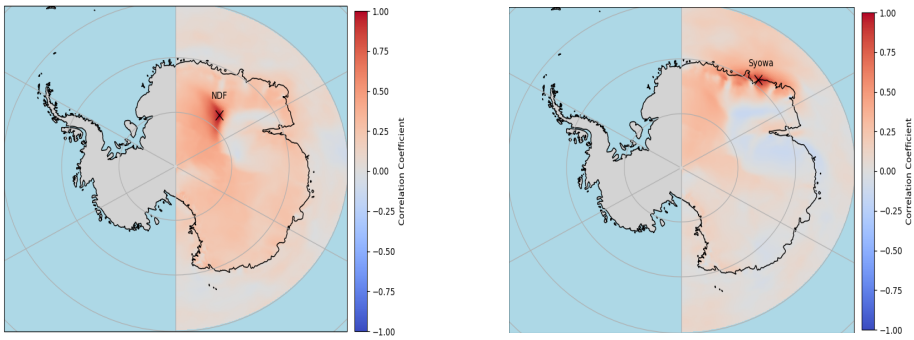

Figure 1. Spatial distribution of correlation coefficients in East Antarctica in 2022. (Left) Based on the NDF site, (Right) Based on Syowa Station.

References

Kotake T, Sugiura K, Hirasawa N, Motoyama H, Hori M, Seasonal variations in wind speed and wind direction at the top of the Antarctic ice sheet. Summaries of JSSI & JSSE Joint Conference on Snow and Ice Research - 2024 in Nagaoka, 2024.

Kotake T, Sugiura K, Hori M, Hirasawa N, Spatiotemporal variations in wind patterns over the western region of East Antarctica. Summaries of JSSI & JSSE Joint Conference on Snow and Ice Research - 2025 in Tsu, 2025.

OMp13

Investigating diamond dust formation under ice supersaturation: observational insights from Fairbanks, Alaska and validation of particle size distribution models

S. Oki[1], K. Sugiura[2], M. Hori[2], H. Iwata[3], and M. Ueyama[4]
[1]*Graduate School of Science and Engineering, University of Toyama, Japan*
[2]*Faculty of Sustainable Design, University of Toyama, Japan*
[3]*Department of Environmental Science, Shinshu University, Japan*
[4]*School of Environmental Sciences and Technology, Osaka Metropolitan University, Japan*

Diamond dust refers to a type of fog (ice fog) composed of ice crystals that forms near the ground in cold regions. It is particularly called this because the ice crystals reflect light, creating a sparkling effect (The Japanese society of snow and ice, 2014). It is generally known that global warming is particularly pronounced in the Arctic. To verify whether existing particle size distribution models for ice fog (Huffman and Ohtake, 1972) can be applied to diamond dust, which can be observed in cold environments and is considered an indicator of climate change, field observations were conducted in Fairbanks, Alaska, at the end of 2024.

Field observations were conducted from November 18 to December 6, 2024, and diamond dust was observed twice during this period (Case 1: 12:30 p.m. on November 19, Case 2: 11:15 a.m. on November 27). In both cases, the air temperature had dropped monotonically from the previous day by approximately 15 K (Case 1) and approximately 19 K (Case 2), and the atmosphere was supersaturated with ice at the time of observation (Figure 1). On the other hand, there were also dates and times when diamond dust was not observed despite the atmosphere being supersaturated with ice (Figure 1). In this study, particle size distribution was calculated using a model proposed by a previous study (Huffman and Ohtake, 1972) that constructed a particle size distribution model for ice fog based on observations conducted in Fairbanks, Alaska, the same location as the current field observation site. The results showed that particle size varied with the number of ice crystals generated per unit time per unit volume. At 700 s^{-1} m^{-3}, the median particle size distribution was approximately 200 μm, which is the typical size of diamond dust. Based on these results, we expect to be able to reproduce the conditions under which diamond dust occurs in greater detail by examining the model parameters for ice crystal nucleation and growth processes and further evaluating the consistency between observations and the model.

This work was a part of the Overseas Fellowship Program, Arctic Challenge for Sustainability II (ArCS II) Project.

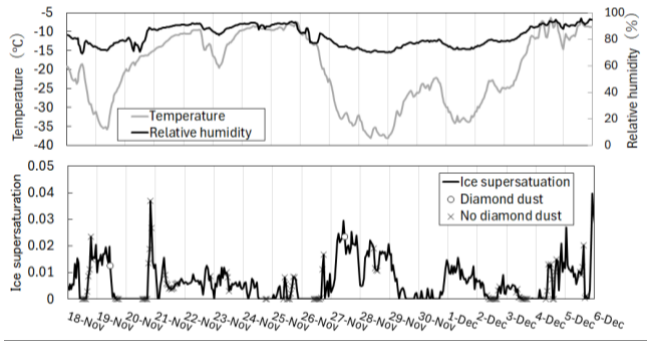

Figure 1. Time series data for Fairbanks from November 18 to December 6, 2024. (a) Air temperature and relative humidity, (b) ice supersaturation. Circles indicate diamond dust observations, while x's indicate cases where diamond dust was not observed.

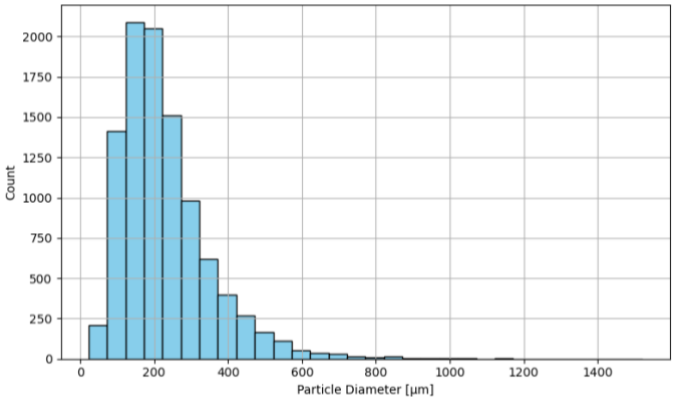

Figure 2. Ice crystal size distribution adjusted for the observation conditions of this study based on previous research.

References

The Japanese society of snow and ice, Japanese dictionary of snow and ice, 2nd edition, Kokon Shoin, 115, 2014.
Huffman PJ and Ohtake T, Formation and growth of ice fog particles at Fairbanks, Alaska. Journal of geophysical research, 76, 657-665, 1972.

OMp14

Solar activity cycle component in variations of snow cover distribution in the Northern Hemisphere

Masahiro Hori[1], Masashi Niwano[2], Rigen Shimada[3], Teruo Aoki[2]

[1]*University of Toyama*
[2]*Meteorological Research Institute*
[3]*Japan Aerospace Exploration Agency*

In the Arctic region, rising temperatures and decreasing sea ice extent have been reported in recent years due to Arctic Amplification. Regarding snow cover area in the Northern Hemisphere, analysis of satellite-borne optical sensor data by the authors revealed a continuous decline trend across all seasons since 1978. Notably, in Europe, the seasonal snow cover duration (SCD) has significantly shortened over the past 40 years. Subsequent investigations also found areas in North America where SCD has lengthened since the 21st century. Correlation analysis between SCD and the Arctic Oscillation Index (AOI) revealed that the shortening of SCD in Europe correlated well with AOI, whereas the lengthening of SCD in North America showed no correlation with AOI. Thus, snow distribution exhibits complex responses to recent global warming. As part of exploring SCD variability mechanisms, this study aimed to extract natural variability components in snow cover distribution synchronized with solar activity cycles. Lag correlation analysis (with SSN lagged 0 to -9 years) was performed between sunspot numbers (SSN) and snow cover duration (SCD), snow melt date (SMD), and snow appearance date (SAD) over 42 years (1982–2024). The results revealed that when SSN was lagged by -3 to -4 years, the correlation between SSN and snow distribution was highest across a broad area of the Northern Hemisphere, excluding parts of North America and East Asia. This indicated a tendency for SCD to lengthen (shortening) with increasing (decreasing) sunspot numbers, SMD to be delayed (early), and SAD to be early (delayed). Over the past 40 years, while sunspot numbers have shown a decreasing trend, a significant shortening of SCD has been observed in the region centered on Europe in western Eurasia, consistent with the SSN correspondence. Conversely, in North America, as mentioned earlier, a lengthening of SCD (and an earlier onset of SAD) has been detected since the 21st century, showing signs contrary to the SSN correspondence.

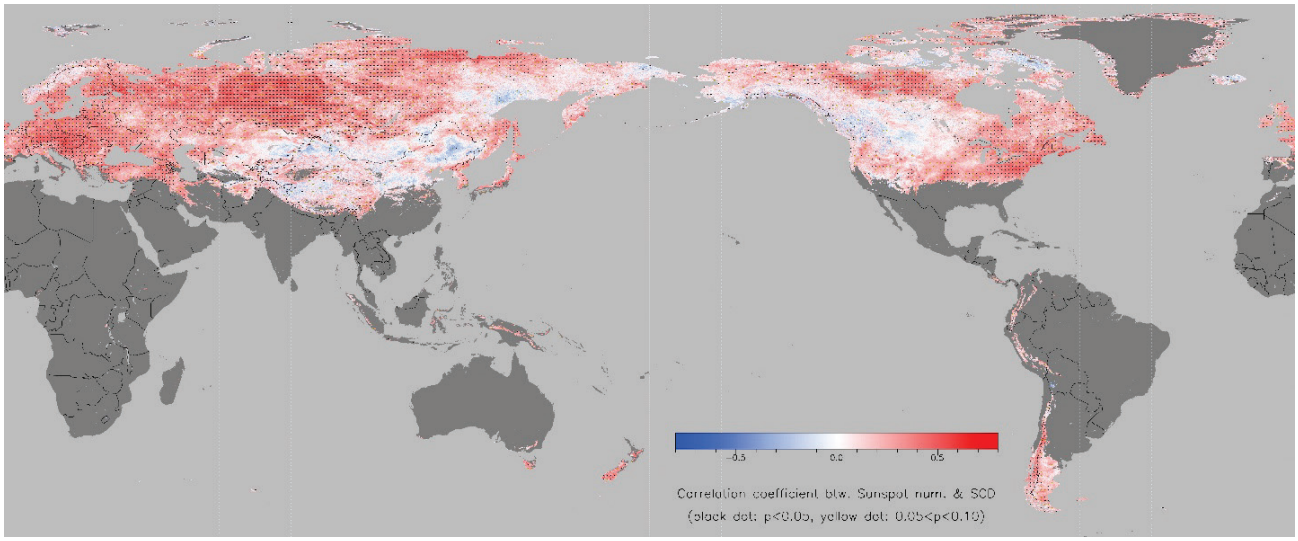

Figure 1. Spatial distribution map of the lag correlation coefficient between sunspot numbers (SSN) and the Northern Hemisphere snow cover duration (SCD) (SSN leads by 3 years) over 42 years (1982–2024). Black and dark yellow dots indicate regions significant at the 5% and 10% significance levels, respectively.

References

IPCC, 2023: Climate Change 2023: Synthesis Report. Contribution of Working Groups I, II and III to the Sixth Assessment Report of the Intergovernmental Panel on Climate Change. IPCC, Geneva, Switzerland, pp. 35-115.

Hori, M. et al., 2017: A 38-year (1978-2015) Northern Hemisphere daily snow cover extent product derived using consistent objective criteria from satellite-borne optical sensors. Remote Sens. Environ., 191, 402-418.

Hori, M. et al. 2024: Can the spatio-temporal distribution of recent snow cover in the Northern Hemisphere be explained by variations in the Arctic Oscillation Index? The 15th Symposium on Polar Science, OMp20.

Exploring classification methods for snow deposition and erosion patterns on the Antarctic ice sheet using machine learning techniques

Konosuke Sugiura[1], and Naohiko Hirasawa[2]
[1]*University of Toyama*
[2]*National Institute of Polar Research*

In Antarctica, katabatic winds blow down from the top of the ice sheet toward the coast. Strong winds on the snow surface frequently cause blowing snow, leading to deposition and erosion. This process forms various patterns on the snow surface. Since snow surface patterns affect the surface mass balance of the ice sheet, we have started classifying snow surface patterns photographed during a transect survey from the Antarctic coast to the top of the ice sheet. Snow surface images were collected along a round-trip route from the Antarctic coast to the top of the ice sheet using snow vehicles. These snow surface images were captured during the JARE59 (summer 2017–2018) and JARE60 (summer 2018–2019) periods. Previous research (Sugiura and Hirasawa, 2023) introduced an evaluation of classification methods for snow accumulation and erosion patterns on the Antarctic ice sheet using machine learning techniques. This study presents an attempt to classify snow accumulation and erosion patterns (sastrugi, large sastrugi, dune, ripple) using the round-trip image data obtained from JARE59 and JARE60.

Figure 1 shows the classification results for the outward leg of JARE59. It reveals how the appearance probabilities of the four snow surface patterns change with elevation. However, compared to the outward leg of JARE59, the inward leg showed different appearance probabilities at each elevation. Furthermore, both the outward and inward legs of JARE60 yielded extremely low appearance probabilities for dunes and ripples. This study explores these issues to improve estimation.

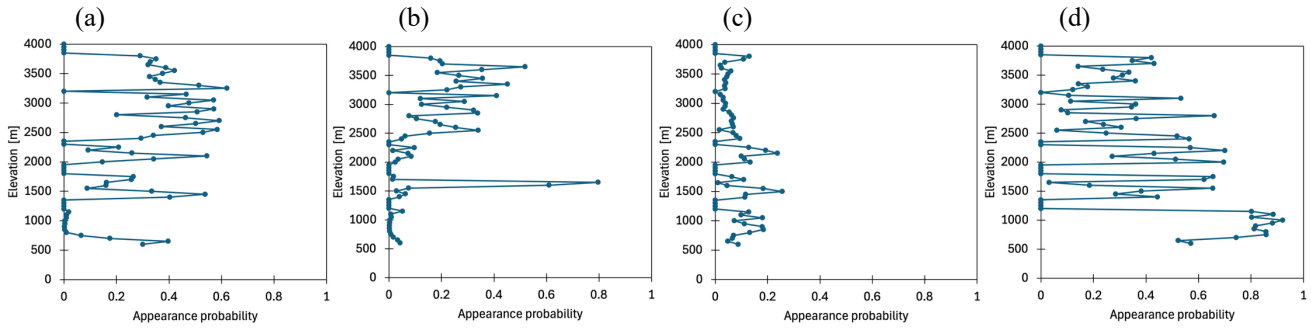

Figure 1. Probability of appearance of snow accumulation and erosion patterns from the Antarctic coast to the top of the ice sheet. (a) small sastrugi, (b) large sastrugi, (c) dune/barchan, and (d) ripple.

References

Sugiura, K. and N. Hirasawa, Evaluation of classification techniques for snow deposition and erosion patterns in the Antarctic ice sheet using a machine learning method, The 14th Symposium on Polar Science, OM-P-16, 2023.

OMp16

Establishing glaciological research program at the Dobrowolski Station, Bunger Hills, East Antarctica

Michal Petlicki[1]
[1]*Institute of Geophysics, Polish Academy of Sciences*

The Bunger Hills, situated on the Shackleton Ice Shelf margin of East Antarctica, are an unusual coastal oasis where exposed bedrock, lakes, and outlet glaciers coexist alongside the grounded ice sheet. Despite being identified as a scientifically valuable site as early as in the 1950s, the region has remained largely overlooked in modern glaciological research. With the recent reactivation of the Dobrowolski Station managed by Poland, there is a renewed opportunity to establish systematic glaciological research in this sector. However, given the logistical constraints of maintaining continuous field operations in such a remote location, the initial phase of our program is based primarily on remote sensing and modelling.

Our research framework integrates multi-sensor satellite observations with numerical simulations. ICESat-2 altimetry and CryoSat-2 radar data are being used to detect elevation and thickness changes, while Sentinel-1 SAR provides velocity fields and grounding line migration estimates. Optical datasets from medium to high resolution satellites support mapping of surface features, including glacier fronts positions and permafrost-related landforms within the oasis. These observational products are coupled with reanalysis data (ERA5) and regional climate models (RACMO2) to reconstruct surface mass balance and snow cover evolution, and with ice-flow modelling experiments to test the sensitivity of outlet glaciers to oceanic and atmospheric forcing.

The overarching aim is to produce the first coordinated baseline of cryospheric processes in the Bunger Hills region. This will not only fill a critical gap in East Antarctic glaciological observations but also contribute to the design of future *in situ* studies once logistics allow for more regular field operations. Establishing Dobrowolski Station as a focal point for this research has strategic value as it contributes to SCAR initiatives on Antarctic ice mass balance, and strengthens international datasets needed to refine global sea-level projections. Early results already suggest localised glacier changes and possible sensitivity to ocean forcing, underlining the scientific potential of reactivated infrastructure in this historically overlooked region of East Antarctica.

OMp17

Characteristics and sources of microparticles in a Kamchatka ice core

Naoko Nagatsuka[1], Kana Nagashima[1] and Sumito Matoba[2]
[1]*JAMSTEC*
[2]*Institute of Low Temperature Science, Hokkaido University*

The subarctic North Pacific is a high-nutrient, low-chlorophyll (HNLC) region, where the phytoplankton growth is limited by the scarcity of trace metals such as iron. In this region, Asian desert mineral dust and combustion-derived particles are considered the major contributors of dissolved iron, accounting for about 40% of the total input (Nagashima et al., 2023). Although combustion-derived iron is emitted in smaller quantities than natural mineral sources, its high solubility makes it an important source of bioavailable iron (Sholkovitz et al., 2009). In addition, volcanic ash from eruptions in the Kamchatka Peninsula has recently been recognized as a new iron source. Volcanic ash rapidly releases iron into seawater, and during large-scale eruptions it can significantly increase surface ocean iron concentrations (Hamme et al., 2010). However, the flux of iron-bearing particles exhibits strong regional and seasonal variability, and their sources and temporal variations remain unclear.

To establish reference information on microparticles transported to this region, we analyzed the size, morphology, and composition of particles preserved in an ice core from Kamchatka (Ichinsky: 55.46N, 157.55W, 3607 m a.s.l) using scanning electron microscopy (SEM) with energy-dispersive X-ray spectroscopy (EDS). This ice core is located on the western margin of the subarctic North Pacific region. Furtheremore, we reconstructed temporal variations in ice-core mineral sources by applying a recently developed provenance-tracing technique, namely SEM-cathodoluminescence (CL) analysis of single quartz particles.

The results showed that the Ichinsky ice core contained mainly silicate minerals, as well as volcanic grass and black carbon (Fig. 1). A detailed discussion will be presented at the symposium.

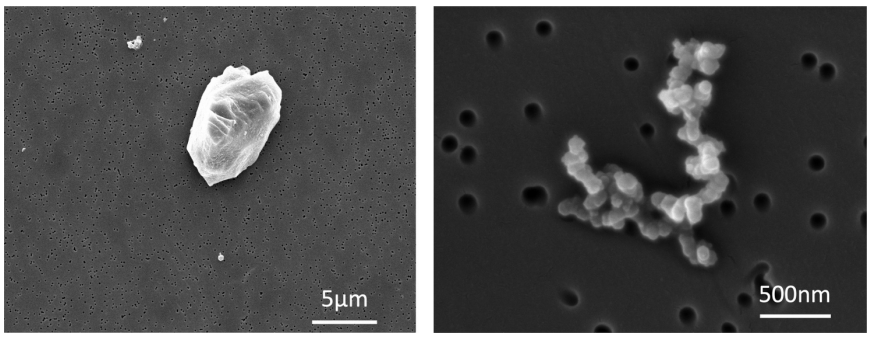

Figure 1. SEM-images of micropartilces in Ichinsky ice core

References

Nagashima K, Kawakami H, Sugie K et al, Asian dust-deposition flux to the subarctic Pacific estimated using single quartz particles. Scientific Report 13, 15424, 2023.

Sholkovitz, ER, Sedwick, PN and Church, TM, On the fractional solubility of copper in marine aerosols: Toxicity of aeolian copper revisited, Geophys. Res. Lett 37, L20601, 2010.

Hamme, RC, Webley, PW, Crawford, WR et al, Volcanic ash fuels anomalous plankton bloom in subarctic northeast Pacific, Geophys. Res. Lett., 37, L19604, 2010.

OMp18

Temporal and spatial changes in mineral dust composition deposited on an alpine snowpack

P. Ataka[1], R. Sugiyama[1] and N. Takeuchi[2]
[1]*Graduate School of Science and Engineering, Chiba University, Japan*
[2]*Graduate School of Science, Chiba University, Japan*

Snow and ice sheets in polar regions, including Greenland and Antarctica, are indispensable components of the Earth's climate system, but they are changing rapidly due to recent climate warming. The frequent occurrence of unseasonal thaws and early snowmelt threatens the stability of these environments. Snowmelt is also enhanced by light-absorbing impurities (LAPs) deposited on the snow surface. Impurities in snowpacks can reduce the surface albedo and increase the absorption of solar radiation, accelerating the melting of the snowpacks (Warren, 1984). Therefore, it is crucial to understand the supply and deposition processes of impurities on snowpacks.

Mineral dust is one of the major light-absorbing impurities in snowpacks. It is usually transported from distant arid regions such as deserts and/or local grounds and deposited on the snowpack surface. Mineral dust also supports the growth of microbes living in snowpacks. For example, photosynthetic microbes called snow algae commonly grow on snowpacks in the Arctic during the melting season, using nutrients supplied by mineral dust for their growth. Therefore, the amount and characteristics of mineral dust can affect microbial activity on the snowpack surface. Since the microbes can also reduce the surface albedo of the snowpacks, mineral dust is likely to have a positive feedback effect on snow melting. However, there is a lack of information on the mineralogical characteristics and transportation processes of mineral dust on the snowpack surface.

In this study, we aimed to describe the temporal and spatial variations in mineral dust on the snowpack surface in an alpine region in Japan. We analyzed the mineralogical composition of the surface dust using X-ray diffraction (XRD) and scanning electron microscopy (SEM) analyses and discussed their sources and effects on surface albedo and microbes of the snowpack.

The XRD analysis identified multiple silicate minerals (quartz, feldspar, chlorite, biotite, and hornblende) and sulfur in all samples (Fig.1). We found that the silicate mineral composition in June and July was significantly different from the April samples, which were dominated by Asian dust (PERMANOVA test, $P < 0.05$). Specifically, the proportion of quartz significantly decreased, while chlorite, biotite, and hornblende significantly increased (Fig.2). This result suggests that the mineral dust on the snowpack was initially composed mainly of Asian dust, but as the snowmelt progressed after May, it was mixed with local sources of mineral particles. Furthermore, the spatial distribution analysis revealed local variations in the abundance of individual mineral species, showing distinct differences depending on the location. Additionally, sulfur showed elevated proportions in the western part of the central study area. Since an active fumarole is located near this region, the high sulfur content suggests that the fumarole is a local source of solid sulfur deposited on the snow surface.

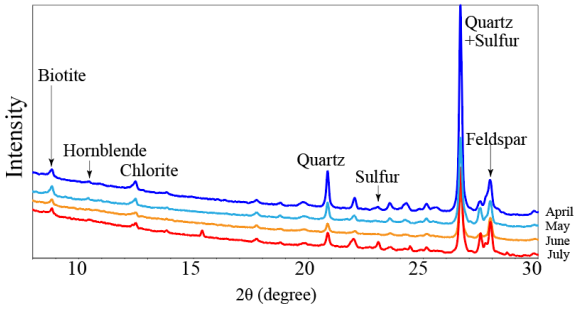

Figure1. Representative XRD patterns of snow samples from April to July.

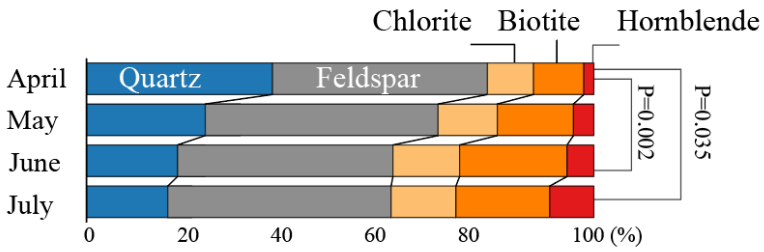

Figure2. Temporal changes in the relative peak intensities of silicate minerals from April to July. Relative peak intensity ratio = intensity of each mineral peak / sum of major mineral peak intensities. P values indicate the results of PERMANOVA tests.

References

Warren, S. G. (1984). Impurities in snow: Effects on albedo and snowmelt. *Annals of Glaciology*, 5, 177–179.

OMp19

Variations in black carbon particle concentrations and sizes during Antarctic Isotope Maxima 8-13 revealed by the Dome Fuji deep ice core

Kumiko Goto-Azuma[1], Kaori Fukuda[1], Jun Ogata[1], Nobuhiro Moteki[2], Tatsuhiro Mori[3], Sho Ohata[4], Yutaka Kondo[5], Makoto Koike[5], Ikumi Oyabu[1, 6], Motohiro Hirabayashi[1], Shuji Fujita[1, 6], Fumio Nakazawa[1, 6] Tomotaka Saruya[1], Kyotaro Kitamura[1], and Kenji Kawamura[1, 6]

[1] *National Institute of Polar Research, Japan*
[2]*Tokyo Metropolitan University, Japan*
[3]*Keio University, Japan*
[4]*Nagoya University, Japan*
[5]*The University of Tokyo, Japan*
[6]*SOKENDAI (The Graduate University for Advanced Studies), Japan*

In recent years, human-induced global warming has led to an increase in large-scale wildfires, floods, heatwaves, and droughts, raising concerns that the Earth's climate system may be approaching or surpassing tipping points. However, the conditions under which tipping points are crossed, as well as the nature and pace of the resulting climatic and environmental changes, remain poorly understood. This knowledge gap hampers our ability to estimate their impacts on society and the economy and to devise effective countermeasures.

Studies of Greenland ice cores have revealed 25 abrupt climate shifts during the last glacial period, known as Dansgaard–Oeschger (DO) events, during which mean annual temperature rose by as much as 10 °C within only a few decades (numbered DO1–DO25 in chronological order). Corresponding Antarctic warming events, termed Antarctic Isotope Maxima (AIM), have also been identified in Antarctic ice cores. Because DO events and AIM occurred in the absence of human influence, they are regarded as evidence that the climate system crossed tipping points in the past. High-resolution analyses of Greenland and Antarctic ice cores therefore provide valuable insights into the mechanisms and consequences of such rapid warming events. We are investigating climatic and environmental changes during DO events and AIM through high-resolution analyses of ice cores from the East Greenland Ice-core Project (EGRIP) and Dome Fuji (DF), Antarctica. In this presentation, we report on variations in the concentration and size of black carbon (BC) in the Dome Fuji ice core associated with AIM, which provide evidence for past changes in biomass burning.

We analysed the second DF deep ice core over a depth interval between 730 and 930 m, corresponding to AIM 8–13, using a Continuous Flow Analysis (CFA) system developed at the National Institute of Polar Research. The CFA system enabled us to obtain high-resolution records of BC, stable water isotopes, microparticles, and eight elements (Na, Mg, Al, Si, K, Ca, Fe, and S). For BC analysis, we employed a Wide-range Single Particle Soot Photometer (WR-SP2; Mori et al., 2016), which can detect BC particles with diameters ranging from 70 to 4000 nm. The combination of WR-SP2 with a high-efficiency nebuliser allowed accurate determination of both concentrations and size distributions of BC particles.

We calculated BC mass flux from BC concentration and accumulation rate data. The BC mass flux increased by a factor of two during the relatively cold interval between AIM 8 and AIM 12 compared with the warmer intervals around AIM 8 and AIM 12. In contrast, no clear change was observed between the end of AIM 14 and AIM 12. The average mass of BC, an indicator of BC particle size, was two- to threefold higher between AIM 8 and AIM 12, but remained lower during other periods. These findings suggest that biomass burning in the continents surrounding the Southern Ocean did not respond to smaller AIM events.

Reference

Mori, T. et al., Improved technique for measuring the size distribution of black carbon particles in liquid water, Aerosol Science & Technology, 50, 3, 242-254, DOI: 10.1080/02786826.2016.1147644, 2016.

OMp20

Local and remote source dust variations at EGRIP, northeastern Greenland

Yuki Komuro[1,2], Fumio Nakazawa[1,3], Kumiko Goto-Azuma[1,3], Naoko Nagatsuka[4], Motohiro Hirabayashi[1], Jun Ogata[1], Kaori Fukuda[1], Naoyuki Kurita[5], Koji Fujita[5], Ayaka Yonekura[6], Kyotaro Kitamura[1], Giulia Sinnl[7], Sune Olander Rasmussen[7], Trevor James Popp[7] and Dorthe Dahl-Jensen[7]

[1]*National Institute of Polar Research*
[2]*Laboratory for Environmental Research at Mount Fuji*
[3]*The Graduate University for Advanced Studies, SOKENDAI*
[4]*Japan Agency for Marine-Earth Science and Technology*
[5]*Nagoya University*
[6]*Marine Works Japan*
[7]*University of Copenhagen*

The Greenland ice sheet likely receives mineral dust from remote arid regions (e.g., Asian deserts) and from local soil regions (e.g., coasts in Greenland). Recent coastal ice-core studies in Greenland have reported an increase in mineral dust from the coasts, driven by shrinking snow cover and expanding soil exposure associated with recent warming (Nagatsuka et al., 2021; Amino et al., 2021). However, few studies have focused on coastal-source mineral dust in the Greenland ice sheet interior, and its variability remains unclear. In this study, we analyzed a shallow ice core drilled at the East Greenland Ice Core Project (EGRIP) site to reconstruct the variations in mineral dust from remote and local sources in the ice sheet interior and to examine the drivers of these variations.

We analyzed the entire depth of the ice core using the continuous flow analysis (CFA) system at the National Institute of Polar Research. Concentrations of eight elements (Na, Mg, Al, Si, S, K, Ca, Fe) were measured using an ICP-MS (7700, Agilent Technologies) connected to the CFA system. A portion of the meltwater was collected with a fraction collector and analyzed with a Coulter counter (Coulter Multisizer 4e, Beckman Coulter) to determine the size-resolved concentrations of mineral dust (0.7–10 μm). For tritium analysis, ice samples from 13–15 m depth were subsampled, melted, and analyzed using a liquid scintillation counter (Quantulus 1220, PerkinElmer). Snow-cover fraction data were derived from the ECMWF reanalysis dataset (ERA5-Land).

Based on annual layer counting, volcanic layers, tritium peaks, and ice layers, the ice core was estimated to cover the past 1000 years. The Coulter counter analysis showed that the average size distribution of mineral dust was unimodal with a mode around 2 μm, suggesting that most of the mineral dust transported to EGRIP originated from remote sources. The concentration of coarse mineral dust (>5 μm), which mainly originates from the coasts in Greenland, varied on decadal scales since 1900 but remained low since 1990s. The absence of increasing coarse dust concentration since 2000 contrasts with increasing dust emissions along the coasts associated with decreasing snow cover during the same period. To investigate the causes of variability in coarse dust concentration, we calculated the contribution of air masses originating from the coasts using back-trajectory analysis. The temporal variation of the contribution was inconsistent with that of coarse dust concentration if considering only air-mass transport; however, the two showed similar temporal trends if snow-cover fractions at the ground surface were also considered in the calculation. This suggests that the mineral dust supply from the coasts to EGRIP was affected not only by the area of exposed soil but also by atmospheric conditions over Greenland. The coarse dust concentration showed a significant correlation with the Greenland blocking index, suggesting that these atmospheric conditions were related to the strength of the high-pressure system around Greenland. In our presentation, we will also report on results concerning mineral dust from remote sources.

References

Nagatsuka et al., Variations in mineralogy of dust in an ice core obtained from northwestern Greenland over the past 100 years, Climate of the Past, 17(3), 1341-1362, 10.5194/cp-17-1341-2021, 2021.
Amino et al., Increasing dust emission from ice free terrain in southeastern Greenland since 2000, Polar Science, 27, 100599, 10.1016/j.polar.2020.100599, 2021.

OMp21

$\delta O_2/N_2$ measurement in the bubble-clathrate hydrate transition zone of the Dome Fuji ice core

Munehiro Asao[1], Ikumi Oyabu[1,2] and Kenji Kawamura[1,2]

[1] *The Graduate University for Advanced Studies*
[2] *National Institute of Polar Research*

Polar ice cores provide valuable information about paleoclimate, which allow us to understand the mechanisms of climate change. Precise ice core chronologies are essential for determining the timing and duration of climatic events. Annual layer counting using seasonal varying parameters is suitable for ice cores from high-accumulation sites (e.g., Svensson et al., 2008). However, it is not possible to identify annual layers for ice cores from low-accumulation sites such as Antarctic interior. The age scales of deep ice cores at low-accumulation sites are tipically constructed by ice flow model and accumulation model constrained with various age markers. For constraining old layers, orbital tuning is commonly employed, in which measured parameters (e.g., $\delta O_2/N_2$, $\delta^{18}O_{atm}$, total air content) are aligned to Earth orbital parameters as targets. Variation of $\delta O_2/N_2$ at Dome Fuji (DF) are highly correlated with the variation of local summer insolation and suitable for orbital dating (Kawamura et al., 2007; Oyabu et al., 2022). During the close-off process occuring at the bottom of firn, relatively small molecules such as O_2 are preferentially excluded from bubbles to open pores (Severinghaus and Battle, 2006; Huber et al., 2006). Therefore, $\delta O_2/N_2$ variations are considered to reflect the physical properties of snow during the densification process, which are strongly influenced by summer insolation (Fujita et al., 2009).

In the latest DF core chronology (DF2021, Oyabu et al., 2022), $\delta O_2/N_2$-based tie points are placed every 10 kyr below 1400 m, where no other age markers are available. However, between 800- 1200 m in the bubble-clathrate hydrate transition zone (BCTZ; 450-1200 m at Dome Fuji) and just below it (1200-1400 m), the $\delta O_2/N_2$ values show large scatter. As a result, $\delta O_2/N_2$ tie points are unavailable between 800 and 1400 m and the largest ice age uncertainty (±2400 yr) exists at 1000-1200 m in DF2021.

Microscopic obserbations by Ohno et al. (2004) found layered distributions of bubble and hydrates on a few-milimeter scale in the BCTZ. Ikeda-Fukazawa et al. (2001) analyzed $\delta O_2/N_2$ of indivisual bubbles and hydrates by Raman spectroscopy and found extreme fractionation between bubbles and hydrates; up to +1000 ‰ for hydrates and -740 ‰ for bubbles. Based on these studies, Oyabu et al. (2021) proposed a hypothesis that the large $\delta O_2/N_2$ scatter in the lower BCTZ is caused by the extreme fractionation of $\delta O_2/N_2$ on millimeter scale and random inclusion of bubbles and hydrates at the top and/or bottom of the sample. They also suggested that analyzing longer samples could reduce such scatter.

In this study, we analyzed 50-cm-long ice core samples for $\delta O_2/N_2$ to test whether the longer samples indeed reduce the scatter in the lower BCTZ and reproduce the variation of $\delta O_2/N_2$ suitable for the orbital tuning. We plan to analyze 120 samples of the 1st DF ice core between 750-1150 m (corresponding to 40-70 kyr BP, 500 yr-time resolution on average), where the largest scatter was found by Oyabu et al. (2021). In this symposium, we report the initial results of 5 samples between 750- 850 m and 14 samples between 1050- 1150m.

We cut out 50-cm ice samples (about 50 g) from bulk cores (~50 cm). All sample surfaces were removed by the thickness of >1 cm to eliminate the fractionation by gas loss during storage (the sample length becomes ~48 cm). We split the sample into 4 pieces (each segment was 12-cm long) and put in 4 different vessels to analyze the variation within the sample. To avoid the loss of fractionated layers between the neighboring 12-cm samples, we did not cut samples with a band saw but broke them with fingers, by which the sample masses did not decrease.

The methods for air extraction and measurement follow Oyabu et al. (2020). Beriefly, an ice sample was melted in an evaculated vessel, and the released air was immediately transferred to a sample tube. The air sample was measured with a mass spectrometer (Thermo Delta V) for $\delta O_2/N_2$ and $\delta^{15}N$.

Around 1100 m, the 50-cm average $\delta O_2/N_2$ show smaller scatter (1σ = 1.7 ‰) than the published data (1σ = 6.1 ‰) with 11-cm samples (Oyabu et al., 2021), and they are close to the values expected from the local summer solstice insolation curve scaled to the $\delta O_2/N_2$ data in the clathrate zone (Oyabu et al., 2021). On the other hand, the $\delta O_2/N_2$ variability calculated using the 12-cm values (1σ = 5.3 ‰) is comparable to the previous data (Oyabu et al.,

2021). Moreover, alternating high and low values around the average are found for some samples, consistent with the hypothesis of Oyabu et al. (2021). On the other hand, $\delta O_2/N_2$ around 800 m are considerably higher than the value expected from the scaled local insolation curve. We suggest that the values are affected by artefacts of the fact that air exists mainly as bubbles in this depth range (Ohno et al., 2004), in combination with $\delta O_2/N_2$ being lower in bubbles than in clathrates (Ikeda-Fukazawa, 2001). The bubble air near the sample surface with low $\delta O_2/N_2$ is more prone to be lost during the sample cutting and shaving, biasing the extracted air towards higher $\delta O_2/N_2$.

In conclusion, the $\delta O_2/N_2$ could be reconstructed to place useful age tie points in the bubble-clathrate transition zone, by analyzing more samples of 50-cm long as proposed by Oyabu et al. (2021).

References

Fujita, S., Okuyama, J., Hori, A., Hondoh, T.,Metamorphism of stratified firn at Dome Fuji, Antarctica: A mechanism for local insolation modulation of gas transport conditions during bubble close off. . J. Geophys. Res. 114, 2008JF001143 2009.

Huber, C., Beyerle, U., Leuenberger, M., Schwander, J., Kipfer, R., Spahni, R., Severinghaus, J., Weiler, K.,Evidence for molecular size dependent gas fractionation in firn air derived from noble gases, oxygen, and nitrogen measurements. . Earth and Planetary Science Letters 243, 61–73 2006.

Ikeda‐Fukazawa, T., Hondoh, T., Fukumura, T., Fukazawa, H., Mae, S.,Variation in N2 /O2 ratio of occluded air in Dome Fuji antarctic ice. . J. Geophys. Res. 106, 17799−17810 2001.

Kawamura, K., Parrenin, F., Lisiecki, L., Uemura, R., Vimeux, F., Severinghaus, J.P., Hutterli, M.A., Nakazawa, T., Aoki, S., Jouzel, J., Raymo, M.E., Matsumoto, K., Nakata, H., Motoyama, H., Fujita, S., Goto-Azuma, K., Fujii, Y., Watanabe, O.,Northern Hemisphere forcing of climatic cycles in Antarctica over the past 360,000 years. . Nature 448, 912–916 2007.

Ohno, H., Lipenkov, V.Y., Hondoh, T.,Air bubble to clathrate hydrate transformation in polar ice sheets: A reconsideration based on the new data from Dome Fuji ice core. . Geophysical Research Letters 31, 2004GL021151 2004.

Oyabu, I., Kawamura, K., Buizert, C., Parrenin, F., Orsi, A., Kitamura, K., Aoki, S., Nakazawa, T.,The Dome Fuji ice core DF2021 chronology (0–207 kyr BP). . Quaternary Science Reviews 294, 107754 2022.

Oyabu, I., Kawamura, K., Kitamura, K., Dallmayr, R., Kitamura, A., Sawada, C., Severinghaus, J.P., Beaudette, R., Orsi, A., Sugawara, S., Ishidoya, S., Dahl-Jensen, D., Goto-Azuma, K., Aoki, S., Nakazawa, T.,New technique for high-precision, simultaneous measurements of CH4, N2O and CO2 concentrations; isotopic and elemental ratios of N2, O2 and Ar; and total air content in ice cores by wet extraction. . Atmospheric Measurement Techniques 13, 6703–6731 2020.

Oyabu, I., Kawamura, K., Uchida, T., Fujita, S., Kitamura, K., Hirabayashi, M., Aoki, S., Morimoto, S., Nakazawa, T., Severinghaus, J.P., Morgan, J.D.,Fractionation of O2/N2 and Ar/N2 in the Antarctic ice sheet during bubble formation and bubble–clathrate hydrate transition from precise gas measurements of the Dome Fuji ice core. . The Cryosphere 15, 5529–5555 2021.

Severinghaus, J., Battle, M.,Fractionation of gases in polar ice during bubble close-off: New constraints from firn air Ne, Kr and Xe observations. . Earth and Planetary Science Letters 244, 474–500 2006.

Svensson, A., Andersen, K.K., Bigler, M., Clausen, H.B., Dahl-Jensen, D., Davies, S.M., Johnsen, S.J., Muscheler, R., Parrenin, F., Rasmussen, S.O., Rothlisberger, R., Seierstad, I., Steffensen, J.P., Vinther, B.M.,A 60 000 year Greenland stratigraphic ice core chronology. . Clim. Past 2008.

OMp22

Densification of firn-ice transition area and integrated densification model at an inner plateau on an ice sheet in polar regions

Toyoyama, Takako[1,2]

1 Graduate school of Environmental Science, Division of cryosphere science, Hokkaido University

2 Institute of Low Temperature Science, Hokkaido University

At an inner plateau on an ice sheet in polar regions, accumulating snow gradually constructs firn structure with layers of each year. Firn and ice area in an ice sheet as a densification model are divided to three parts as Shallow firn, Firn-ice transition and ice area in this research. The study points out initial air pressure as saturated air pressure, load pressure, densification strain, and ice flow. The densification at the firn-ice transition area studied with the effect of initial air pressure. Main mechanisms of the densification are re-arrangement, sintering, and plastic deformation. Firn-ice transition area keeps air of firn surface in polarity between ice particles. Air is fixed in air bubbles and changing cylindrical shape to sphere for enduring load pressure with increasing density. The density is named 'ice density' on this research. The densification mechanism is plastic deformation with increasing inside air pressure by shrinking volume in an air bubble against load pressure. The relationship of load pressure, initial air pressure and temperature can express as equations of densification strain rate from the experimental-set. Perpendicular strain rate from firn and ice and horizontal flow rate as volume transformation from ice and firn flow law express as scholar of flow dynamics in ice sheet of three parts as shallow firn, firn-ice transition area, and ice.

The equation-set estimates densification and ice flow at ice sheet plateau by integrating densification on shallow firn, firn-ice transition and ice area. Densification at firn-ice transition area divides to three mechanisms on the experimental-set. The main first mechanism is re-arrangement, sintering and fracture. The main second mechanisms is sintering and plastic deformation with air bubbles of cylindrical shape through boundaries of ice particles. At the end of second mechanisms, air bubbles become to sphere shape for enduring load pressure. The main third mechanism is plastic deformation to shrink an air bubble. Inside air pressure in air bubbles becomes like against driving force on densification of load pressure. Experimental densification equations apply to perpendicular densification and horizontal flow in firn and ice. Ice layer as one part of whole densification process at ice plateau or ice cap on inner antarctica follows to ice flow law without adding to effects of friction of base and sides. The densification experiment with effect of initial air pressure on firn surface gives parameters on initial air pressure, 100 kPa, 50 kPa in the sampler. These air pressures are at sea level and about 4000 m altitude at plateau in polar regions. Air pressures, 1 kPa and 0.1 kPa are setting on ice moons around a planet. At low temperature room is 263 K. Firn-ice transition area at ice cap and plateau on inner ice sheet exists on quasi three axis condition. The condition maintains load pressure from firn and ice themselves, and around pressure with strong connection on densification mechanisms in firn as similar with perpendicular compress as quasi three axis compaction.

Load pressure after reaching at ice density increases with deeper depth. Ice layer mainly follows to flow law of flow body with plastic deformation like one axis compaction. The quasi three axis experimental-set indicates to the effect of initial air pressure. Densification strain rate is faster when initial air pressure is lower. The ice density reaches to high density for sintering is not growing much when initial air pressure is lower. The relationship of parameters integrate to densification model at whole ice sheet including shallow firn, firn-ice transition area and ice.

References

Toyoyama, T., The effect of an initial air pressure on firn densification process, **Master thesis**, *Graduate school of Earth Environmental Science in Hokkaido University*, 1998.

OMp23

Monitoring subsurface ice structures in the Greenland Ice Sheet using satellite-based microwave radiometry

Takumi Suzuki[1], Rigen Shimada[1], Misako Kachi[1] and Tomonori Tanikawa[2]
[1]*Japan Aerospace Exploration Agency, Earth Observation Research Center*
[2]*Meteorological Research Institute*

The accelerated melting of the Greenland Ice Sheet has raised concerns about its impact on global sea-level rise. One significant factor contributing to this phenomenon is the formation of dense refrozen ice layers (ice slabs), which inhibit the vertical percolation of surface meltwater and thus enhance runoff (MacFerrin et al., 2019). Accurately mapping the distribution of ice slabs is essential for improving predictions of future meltwater production and its potential impact on sea levels. Previous studies have employed airborne radar and synthetic aperture radar (SAR) to detect ice slabs (Culberg et al., 2024); however, these methods generally suffer from low temporal resolution, limiting their effectiveness. Therefore, developing a method that allows for broad spatial coverage and frequent observations is crucial.

We propose a satellite-based microwave radiometry approach to detect subsurface ice structures in the Greenland Ice Sheet. Using winter-season brightness temperature data (October–April, 2012/13–2024/25) from AMSR2 onboard GCOM-W, we analyzed the difference between 6.9 and 7.3 GHz (ΔTb = Tb(6.9) – Tb(7.3)) for vertical polarization during descending passes. These close frequencies have slightly different penetration depths under dry-snow conditions, allowing us to infer subsurface features. The 6.9 GHz signal is more sensitive to deeper layers, while 7.3 GHz reflects shallower conditions, enabling regional characterization of subsurface ice.

The results show that ΔTb was positive in upstream and peripheral downstream regions across all years, while the midstream region consistently exhibited negative values (Figure 1). In upstream regions, positive ΔTb indicates strong emission from deep refrozen ice layers detected by the 6.9 GHz channel, which penetrates deeper than 7.3 GHz and senses high-emissivity ice slabs beneath porous firn. This signal weakened over time, likely due to surface accumulation elevating the emission layer and reducing the influence of deep ice. In contrast, midstream regions lack dense ice slabs and exhibit a vertical temperature gradient, where relatively warmer shallow firn sensed by 7.3 GHz overlies colder deep layers sensed by 6.9 GHz, resulting in negative ΔTb. In downstream bare-ice regions, positive ΔTb is driven by near-surface structures such as refrozen layers and exposed ice, with interannual variability linked to melt–refreeze cycles and surface lowering.

Our results suggest that satellite-based microwave radiometry can consistently capture the broad-scale distribution and interannual variability of Greenland's subsurface ice structures, offering a promising pathway toward long-term monitoring.

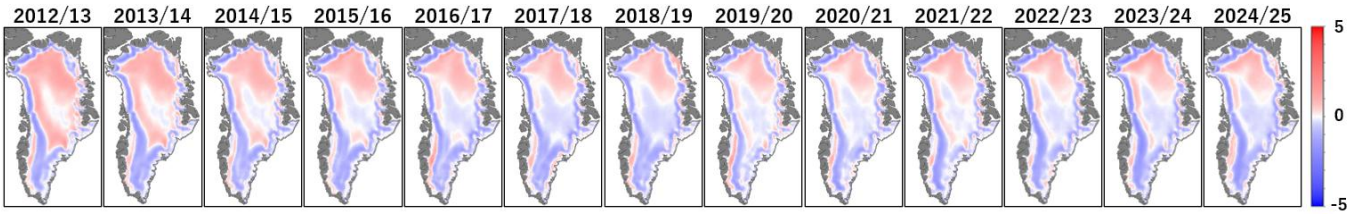

Figure 1. Figure 1. Interannual variation of brightness temperature difference (ΔTb = Tb(6.9) – Tb(7.3)) observed by GCOM-W/AMSR2 over the Greenland Ice Sheet for vertical polarization during descending passes in winter (October–April).

References

MacFerrin M, Machguth H, van As D et al., Rapid expansion of Greenland's low-permeability ice slabs. Nature, 573, 403-407, 2019.

Culberg R, Michaelides RJ, Miller JZ, Sentinel-1 detection of ice slabs on the Greenland Ice Sheet. The Cryosphere, 18, 2531-2555, 2024.

OMp24

Shortwave penetration Drives Subsurface Warming and Melt on the Langhove Glacier, East Antarctica

Jun Saito[1] and Masahiro Minowa[1]

[1]*Institute of Low Temperature Science, Hokkaido University*

Surface meltwater on ice shelves, together with runoff from upstream grounded ice, can pond and drain into crevasses, raising water pressure and promoting hydrofracturing (Kuipers Munneke et al., 2014). Many supraglacial lakes over Antarctic ice shelves are observed during the melt season. This results from surface meltwater production on ice shelves as air temperature increases; discharge from upstream grounded ice is also a major source. However, the timing of formation and downstream release is still unclear. On the Langhovde Glacier in East Antarctica, numerous supraglacial lakes occur up to ~670 m a.s.l. (Langley et al., 2016). They often form on blue ice, which refreezes in early December and then begins to drain a few weeks later. Previous studies in Dronning Maud Land reported subsurface lakes beneath bare ice (Winther et al., 1996) since shortwave radiation can penetrate more deeply, especially in blue ice (Liston et al., 2025). In contrast, nighttime longwave emission removes heat from the surface and can lead to rapid refreezing. To better understand the seasonal evolution of ice thermal structure, we measured ice temperature just upstream of the grounding line on Langhovde Glacier from January 2024 to January 2025(Fig. 1a). The wetting front reached ~2 m depth even though air temperature was below 0 °C for most of the period (Fig. 1 b and c). Observed near-surface ice temperature was ~5 °C higher than that computed by a 1-D heat-transfer model that includes phase change (latent heat) but excludes shortwave-radiation penetration, forced with the observed surface temperature (Fig. 1b). At 14 m depth, ice temperature was ~−6 °C, about 4 °C warmer than the site's mean air temperature. These observations are consistent with shortwave penetration in blue-ice areas driving subsurface warming and temporary storage, with a lagged release of meltwater toward the ice shelf.

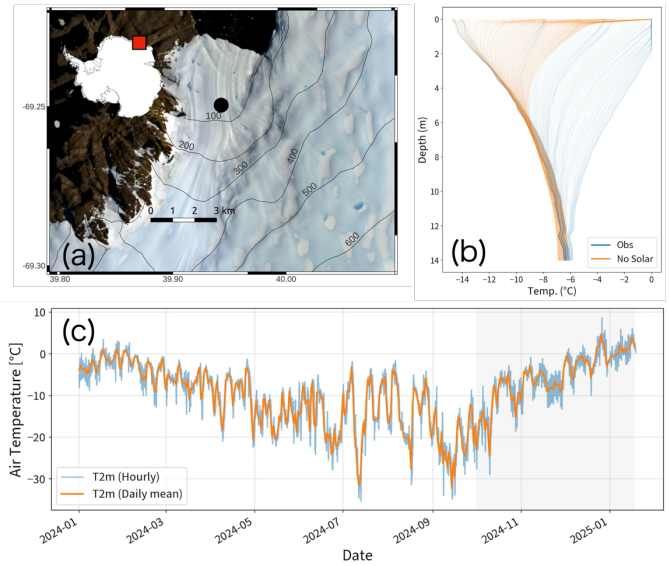

Fig. 1 (a) Location of the Langhovde Glacier study site. (b) Measured ice temperature profile compared with the model output. (c) ERA5 air temperature at the site (black circle). The gray hatched interval (1 Oct 2024–18 Jan 2025) marks the period for which the temperature profile and model output are plotted as (b).

References

Kuipers Munneke P, Ligtenberg SRM, Van Den Broeke MR, Vaughan DG. Firn air depletion as a precursor of Antarctic ice-shelf collapse. *Journal of Glaciology*. 2014;60(220):205-214. doi:10.3189/2014JoG13J183

Langley, E. S., Leeson, A. A., Stokes, C. R., & Jamieson, S. S. R.. Seasonal evolution of supraglacial lakes on an East Antarctic outlet glacier. Geophysical Research Letters, 2016; 43, 8563–8571. https://doi.org/10.1002/2016GL069511

Liston, G. E., and J.-G. Winther, Antarctic surface and subsurface snow and ice Melt Fluxes, J. Clim., 2005; 18(10), 1469–1481, doi:10.1175/ JCLI3344.1.

Winther J-G, Elvehøy H, Bøggild CE, Sand K, Liston G. Melting, runoff and the formation of frozen lakes in a mixed snow and blue-ice field in Dronning Maud Land, Antarctica. *Journal of Glaciology*. 1996;42(141):271-278. doi:10.3189/S0022143000004135

Influence of regridding schemes on coupling between ice-sheet and climate models

SAITO Fuyuki[1], Ryouta O'ishi[2], Takashi Obase[1], Ayako Abe-Ouchi[2] and Wing-Le Chan[2]
[1]*Japan Agency for Marine-Earth Science and Technology(JAMSTEC)*
[2]*Atmosphere and Ocean Research Institute, The University of Tokyo*

Ice sheet evolution is often described as responses to variation of other climate systems such as atmosphere and ocean, however, it is well known that there is interaction between the systems and the changes in ice-sheet do feedback on the other systems. Therefore development of coupling models, which simulate the climate components simultaneously, is an important subject in order to compute the evolution of ice-sheet with high accuracy.

The model domain of global climate models is typically defined on longitude-latitude grid system on a (true) sphere, while that of ice-sheet component is typically defined on regional cartesian grid on polar stereographic projection of a ellipsoid. Exchanges of information between climate and ice-sheet models such as the surface mass balance require a function to absorb the difference of the model structures and, in particular, not to break the conservation. In addition, as already discussed by Fischer et al. (2014), the different structure of the models may cause the projection errors and geometric errors.

In this study, the module adopted in the climate model MIROC to exchange the information between the atmosphere and ocean components (Suzuki et al. 2009) is extended, such that the regional model component of polar stereographic projection can be available. A design to compute polygon areas of overlapped cells follows SPRING (Takeshima et al., 2020) with extending on the polar-stereographic projection. The second-order conservative remapping is implemented using an algorithm presented in Saito (2024).

In the present study, the first- and second-order conservative regridding schemes are applied on a series of typical ice-shee model simulation. The impact on ice-sheet model simulation by difference in the regridding order is demonstrated using ice-sheet model forced by the results of climate model simulation. The result shows that the influence on simulated changes in ice-sheet thickness reflects the feature introduced by assumed local distribution for each souce cell, which may reach 10% of local thickness at 500 simulation year.